Atmos. Chem. Phys. Discuss., https://doi.org/10.5194/acp-2018-720
Manuscript under review for journal Atmos. Chem. Phys.
Discussion started: 3 September 2018

Atmospheric Chemistry and Physics
Open Access
EGU
Discussions

OMI surface UV irradiance in the continental United States: quality assessment, trend analysis, and sampling issues

Huanxin Zhang[1,2], Jun Wang[1,2], Lorena Castro García[1,2], Yang Liu[3], Nickolay A. Krotkov[4]

[1]Department of Chemical and Biochemical Engineering, The University of Iowa, Iowa City, IA, USA
[2]Center for Global and Regional Environmental Research, The University of Iowa, Iowa City, IA, USA
[3]Rollins School of Public Health, Emory University, Atlanta, GA, USA
[4]NASA Goddard Space Flight Center, Greenbelt, MD, USA

Correspondence to: Jun Wang (jun-wang-1@uiowa.edu), Huanxin Zhang (huanxin-zhang@uiowa.edu)

Abstract. Surface full-sky erythemal dose rate (EDR) from Ozone Monitoring Instrument (OMI) at both satellite overpass time and local noon time are evaluated against ground measurements at 31 sites from USDA UV-B Monitoring and Research Program over the period of 2005–2017. We find that both OMI overpass time and local solar noon EDR are highly correlated with the measured counterparts (R = 0.88). Although the comparison statistics are improved with longer time window used for pairing surface and OMI measurements, OMI data overall has ~4% underestimate for overpass EDR while ~8% overestimate for the solar noon time EDR. The biases are analyzed regarding the spatial and temporal data collocation, the effects of solar zenith angle (SZA), clouds and the assumption of constant atmospheric conditions. The difference between OMI overpass EDR and ground observation shows some moderate dependence on SZA and the bias could be up to –30 % with SZA greater than ~65°. In addition, the ratio of EDR between solar noon to overpass time is often (95% in frequency) larger than 1 from OMI products; in contrast, this ratio from ground observation is shown to be normally distributed around 1. This contrast suggests that the current OMI surface UV algorithm would not fully represent the real atmosphere with the assumption of a constant atmospheric profile between noon and satellite overpass times. The viability of surface UV in terms of peak UV frequency is also studied. Both OMI Noon_FS and ground peak EDR show a high frequency of occurrence of ~ 20 mW m^{-2} over the period of 2005–2017. However, another high frequency of ~ 200 mW m^{-2} occurs in OMI solar noon EDR while the ground peak values show the high frequency around 220 mW m^{-2}, implying that the OMI solar noon time may not always represent the peak daily UV values. Lastly, OMI full-sky solar noon EDR shows statistically significant positive trends in parts of the northeastern U.S., the Ohio River Valley region and California. However, the UV trends estimated from ground-based network using two sampling methods (one corresponds to the OMI noon time and one averages all the data in a day) show significant negative trends in the Northeast and the Ohio River Valley region, which is consistent with the increase of absorption aerosol optical depth as revealed by OMI aerosol product in these regions. No statistically-significant trend can be found for OMI columnar O3 or cloud optical depth. The future surface UV data estimated with better spatial and temporal resolution obtained from geostationary satellites would help resolve these discrepancies found in the biases and estimated surface UV trends.

1 Introduction

The amount of surface solar UV radiation (200–400 nm) reaching the earth's surface has substantial impacts on human health and ecosystems (UNEP, 2007; WMO, 2010). For example, about 90 % of nonmelanoma skin cancers are associated with exposure to solar UV radiation in the United States (Koh et al., 1996). Bornman and Teramura (1993) and Caldwell et al. (1995) showed the negative effects of UV radiation on plant growth and tissues. Since the discovery of the significant ozone depletion in the Antarctic region (Farman et al., 1985) and mid latitudes (Fioletov et al., 2002), subsequent effects on surface UV levels have received attention. As a result, great efforts have been made to monitor surface UV radiation from both satellite and ground instruments in the past few decades (Bigelow et al., 1998; Sabburg et al., 2002; Levelt et al., 2006). Although satellite measurements provide a better spatial coverage of the surface UV radiation, they (similar to ground-based observations) are not only affected by instrument errors (Bernhard and Seckmeyer, 1999), but are also subject to uncertainties in the algorithms used to derive surface UV radiation. Therefore, evaluation of satellite-based estimates of surface UV radiation against available ground measurements in many locations around the world is needed to characterize the errors toward further refinement of the surface UV estimates.

The solar spectral irradiance (in mW m^{-2} nm^{-1}) is usually measured by ground and satellite instruments. In addition, the surface UV irradiance, denoted as 'erythmal weighted', has been widely used to describe the sunburning or reddening effects (McKenzie et al., 2004). Erythemally weighted irradiance or erythemal dose rate (in mW m^{-2}) is defined as the incoming solar radiation on a horizontal surface weighted according to the erythemal action spectrum (McKinlay and Diffey, 1987) ; it can be further divided by 25 mW m^{-2} to derive UV index - an indicator of the potential for skin damage (WMO, 2002). Hence, UV index is commonly used as a UV exposure measure to the general public and in epidemiological studies in the U.S. and other parts of the world (Eide and Weinstock, 2005; Lemus-Deschamps and Makin, 2012; Walls et al., 2013). In the U.S., several ground UV monitoring networks have been established responding to changes in the surface UV radiation (Bigelow et al., 1998; Sabburg et al., 2002; Scotto et al., 1988). Currently, the UVMRP initiated by the USDA remains as the only active and largest operating network providing climatological surface UV data in the United States.

The goal of this study is to use UVMRP datasets to evaluate the OMI-based estimates of the surface UV radiation in the past decade in the United States. As a successor of Total Ozone Mapping Spectrometer (TOMS) whose surface UV data (such as erythemally weighted irradiance) has been extensively evaluated in the past (Arola et al., 2005; Cede et al., 2004; Kalliskota et al., 2000; Kazantzidis et al., 2006; McKenzie et al., 2001), the OMI data has a much finer spatial and spectral resolution and thereby bears more advanced capability for characterizing the spatial distribution of the surface UV radiation. TOMS data records span from 1978 to 2005, and many past studies have shown that TOMS surface UV data overestimated the ground observational data in many sites. OMI was launched into space in July 2004 as part of the Aura satellite (Levelt et al., 2006), and it has started to collect data from August 2004 to the present. While there have been a number of studies

Atmos. Chem. Phys. Discuss., https://doi.org/10.5194/acp-2018-720
Manuscript under review for journal Atmos. Chem. Phys.
Discussion started: 3 September 2018

evaluating the OMI surface UV data with ground observations, these studies, as shown in Table 1, have mainly focused on Europe (Antón et al., 2010; Buchard et al., 2008; Ialongo et al., 2008; Kazadzis et al., 2009; Tanskanen et al., 2007; Weihs et al., 2008; Zempila et al., 2016), high latitudes (Bernhard et al., 2015) and the tropics (Janjai et al., 2014). These studies evaluated OMI spectral irradiance, EDR and erythemally weighted daily dose within different time periods. Most comparisons show positive bias up to 69 % with few show negative bias up to –10 %.

This study differs from the past studies in the following ways. Firstly, we conducted a comprehensive evaluation of the OMI surface UV data from 2005 to 2017 covering the continental United States. The evaluation was made for erythemally weighted irradiance at both local solar noon and satellite overpass times, and the evaluation statistics not only concern mean bias but also the probability density function (PDF), cumulative density function (CDF) and variability of the UV data. Secondly, a trend analysis of the surface UV irradiance from both ground observation and OMI was performed, with a special focus on the effects of the temporal sampling. The analysis addresses if the once-per-day sampling from the polar-orbiting satellite would have any inherent limitation for the trend analysis of surface UV data. Finally, the error characteristics in the OMI surface UV data were examined to understand the underlying sources (such as from treatment of clouds and assumption of constant atmospheric conditions between the local solar noon and satellite overpass time). The investigation yields recommendations for future refinement of the OMI surface UV algorithm.

The paper is organized as follows: Sect. 2 describes the satellite and ground observational data; the methodology is discussed in Sect. 3; Sect. 4 presents the results and Sect. 5 summarizes the findings.

2 Data

2.1 OMI data

OMI aboard the NASA Aura spacecraft is a nadir-viewing spectrometer (Levelt et al., 2006) that measures solar reflected and backscattered radiances in the range of 270 nm to 500 nm with a spectral resolution of about 0.5 nm. The 2600 km wide viewing swath and the sun-synchronous orbit of Aura provides a daily global coverage, with an equatorial crossing time at ~ 13:45 local time. The spatial resolution varies from 13 x 24 km^2 (along x cross) at nadir to 50 x 50 km^2 near the edge. OMI retrieves total column ozone, total column amount of trace gases SO_2, NO_2, HOCO, aerosol characteristic and surface UV (Levelt et al., 2006).

The OMI surface UV algorithm has its heritage from the TOMS UV algorithm developed at NASA Goddard Space Flight Center (GSFC) (Eck et al., 1995; Herman et al., 1999; Krotkov et al., 1998; Krotkov et al., 2001; Tanskanen et al., 2006; Krotkov et al., 2002). In the first part of the algorithm, the surface-level UV irradiance at each OMI pixel under clear-sky conditions is estimated from a look-up table that is computed from a radiative transfer model for different values of total column ozone, surface albedo, and SZA. The look-up table was called twice, once to calculate the surface UV irradiance at the satellite overpass time and once at the local solar noon. The only difference between these two look-up tables are the SZAs with one representing the SZAs at the overpass time and the other representing the solar noon, while the total column ozone and cloud optical thickness (COT) are assumed to stay constant. The second step is to correct the clear-sky surface UV irradiance for a given OMI pixel due to the effects of cloud and non-absorbing aerosols. The cloud correction factor is derived from the ratio of measured backscatter irradiances and solar irradiances at 360 nm along with OMI total column ozone amount, surface monthly minimum Lambertian Effective Reflectivity (LER), and surface pressure. The effects of absorbing aerosols are also adjusted in the current surface UV algorithm based on a monthly aerosol climatology as described in Arola et al. (2009).

The second step of the cloud correction mentioned above follows radiative transfer calculations that assume a homogeneous, plane parallel water-cloud model with Rayleigh scattering and ozone absorption in the atmosphere (Krotkov et al., 2001). The COT is assumed to be spectrally independent and the cloud phase function follows the C1-cloud model (Deirmendjian, 1969). This cloud model is also used to calculate the angular distribution of 360 nm radiance at the top of the atmosphere, which is used to derive an effective COT. The effective COT is the same as the actual COT for a homogeneous cloud plane-parallel model. The effective COT is saved to a look-up table to use for cloud correction.

OMI surface UV data products (or OMUVB in shorthand) include: (a) spectral irradiance (mW m^{-2} nm^{-1}) at 305, 310, 324 and 380 nm at both the local solar noon and OMI overpass time, (b) erythemal dose rate (EDR, mW m^{-2}) at both the local solar noon and OMI overpass time and (c) erythemally weighted daily dose (EDD, J m^{-2}). The spectral irradiances assume triangular slit function with full width half maximum of 0.55nm. The EDD is computed by applying the trapezoidal integration method to the hourly EDR with the assumption that the total column ozone and COT remain the same throughout the day. In addition, the OMUVB products include information on data quality related to row anomaly, SZA and COT which are used in the present study. We also use the aerosol products from the OMAERUV algorithm (Torres et al., 2007). The OMI OMAERUV algorithm uses two wavelengths in the UV region (354 and 388 nm) to derive aerosol extinction and absorption optical depth. The aerosol products (OMAERUV) retrieve aerosol optical depth (AOD), aerosol absorption optical depth (AAOD) and single scattering albedo at 354 nm, 388 nm and 500 nm.

In the current study, both OMI level 2 (v003) and level 3 (v003) products are used. The level 2 provides swath level data products while level 3 products are gridded daily products on a 1° x 1° horizontal grid. Two variables from OMUVB level 2 products (Table 2) are used: 1) full-sky solar noon erythemal dose rate denoted as Noon_FS EDR; 2) full-sky overpass time erythemal dose rate denoted as OP_FS EDR. In addition, full-sky solar noon EDR from the OMUVBd (d denotes daily) level 3 products and AOD and AAOD from OMAERUVd level 3 products are used. These level 3 datasets are mainly used for conducting trend analysis in Sect. 4.4 unless noted otherwise while the rest of the data analysis use the level 2 datasets. All the datasets are from January 2005 to December 2017 and row anomaly is checked during data analysis for level 2 datasets.

2.2 Ground observation data

Currently, the UVMRP operates 36 climatological sites for long-term monitoring of surface UV radiation around different ecosystem regions (https://uvb.nrel.colostate.edu/UVB/uvb-network.jsf). Of the 36 climatological sites, five are located in New Zealand, South Korea, Hawaii, Alaska and Canada, while 31 sites are in the continental U.S., with the majority of them located in agricultural or rural areas and a few in urban areas. Among these 31 sites, one site started operation after 2014 and one after 2006, and all other sites started earlier than 2006. In the current study, we use the one site in Canada and 30 of the 31 sites in the continental U.S. and we exclude one site where operation started after 2014 (Fig. 1). All sites measure global irradiance in the UVB spectral range (280–320 nm), using a UVB1-pyranometer manufactured by Yankee Environmental Systems (YES). The YES UVB-1 instrument takes measurement every 15 seconds which are aggregated into 3-min averages. These output data are calibrated following Lantz et al. (1999) and weighted according to McKinlay and Diffey (1987) to generate the erythemally weighted irradiance (300–400 nm). The calibration and characterization of each YES pyranometer were performed annually. The pyranometers differ from the collocated standard triad within ~ ±2.8 % for SZA < 80° and the absolute calibration uncertainty errors could reach ~ ±10 % in some cases when SZA is > 80° (Bigelow et al., 1998; Lantz et al., 1999). In spite of this, McKenzie et al. (2006) has shown that the relative uncertainties could be more important when evaluating the geographical differences in erythemal weighted irradiance at mid-latitude sites maintained by USDA. In this work, we use the 3-min averaged erythemally weighted irradiance at 31 sites in the continental U.S. and information for each site is described in Table 3. Except for site TX41, for which data were available since August 2006, we use data from January 2005 to December 2017 for the rest of the sites.

3 Methods

3.1 Spatial collocation and temporal averaging of data

Since OMI data represent an average over a ground pixel (~13 x 24 km^2 for nadir viewing and ~50 x 50 km^2 for off-nadir viewing) and ground measurements are point measurements that cover a small area, previous work in Table 1 has investigated the effects of the selection of a collocation distance between the center of an OMI ground pixel and the ground observational site or the averaging time period around OMI overpass time/local solar noon on the evaluation results. For example, Weihs et al. (2008) found the variability, defined as the absolute sum of the difference between the average mean bias between OMI and ground measured UV index at any station and the average mean bias from all stations divided by the total number of measurements, increases with increasing collocation distance but decreases with increasing averaging time

Atmos. Chem. Phys. Discuss., https://doi.org/10.5194/acp-2018-720
Manuscript under review for journal Atmos. Chem. Phys.
Discussion started: 3 September 2018

period. Zempila et al. (2016) compared OMI spectral irradiances at 305, 310, 324 and 380 nm with ground observations considering different spatial collocation and temporal averaging windows. It was shown that the choice of collocation distance (10 km, 25 km or 50 km) plays a negligible role in the comparison in terms of the correlation coefficient and mean bias. However, the selection of longer averaging time period (from ± 1 minute to ± 30 minutes) results in a significant improvement under full-sky conditions for both OMI overpass and solar noon time comparison. (Chubarova et al., 2002) evaluated the difference between TOMS overpass surface UV and ground data taken over different time windows around TOMS overpass time. The results showed that the calculated correlation coefficient of these two datasets nonlinearly increases with the increasing averaging windows (from ± 1 minute to ± 60 minutes) and stays nearly constant from ± 60 minutes to ± 90 minutes.

In this work, we will examine the separate effects of spatial collocation and temporal averaging on evaluation results. Firstly, for each ground site, its observation is paired with the OMI data at pixel-level if the center of that pixel is within the distance (D) of 50 km from that ground site. Then the ground observational data at each site is taken within (ΔT of) ± 5 minutes around the OMI overpass time or the local solar noon time at that pixel. Correspondingly, the temporal mean of ground observation within ΔT is compared to the spatial mean of OMI data within D. Further evaluation is conducted by changing different D values to 10 km and 25 km and/or ΔT values of ± 10, ± 30 and ± 60 minutes around OMI overpass time and local solar noon time. Consequently, a total of 12 sets of paired data are generated for the evaluation, as a result of a different combination of three D values and four ΔT values used for spatially and temporally collocating OMI and ground data. For a given ΔT, there are ~ 100,000, ~ 67,000, ~ 17,000 data pairs for D values of 50 km, 25 km and 10 km respectively.

3.2 Validation statistics

First, we present several commonly used validation statistics (Table 2): Mean Bias (MB) calculated in Eq. (1), normalized mean bias (NMB, %) in Eq. (2), the root-mean-square error (RMSE) in Eq. (3) and correlation coefficient (R). We also show the overall evaluation of OMI surface UV data against ground observation in the form of a Taylor Diagram (Taylor, 2001) (see Fig. 3(a)). Taylor Diagram provides a statistic summary of OMI data evaluated against ground observation in terms of correlation coefficient R (the cosine of polar angles), the ratio of standard deviations between OMI and ground observational data (the normalized standard deviation (NSD)) shown in x and y axis respectively, and the normalized room-mean-square difference (RMSD), shown as the radius from the expected point, which is located at the point where R and NSD are unity. The following equations are represented:

$$MB = \frac{1}{N}\sum_{i=1}^{N}(EDR_{(\mathrm{OMI,i})} - EDR_{(\mathrm{Ground,i})}), \quad (1)$$

$$NMB = \frac{\sum_{i=1}^{N}(EDR_{(\mathrm{OMI,i})} - EDR_{(\mathrm{Ground,i})})}{\sum_{i=1}^{N} EDR_{(\mathrm{Ground,i})}}, \quad (2)$$

$$RMSE = \sqrt{\frac{1}{N}\sum_{i=1}^{N}(EDR_{(\mathrm{OMI,i})} - EDR_{(\mathrm{Ground,i})})^2}, \quad (3)$$

Where i is the i-th paired (OMI-Ground) data point, N is the total number of paired data points and $EDR_{(\mathrm{OMI,i})}$ and $EDR_{(\mathrm{Ground,i})}$ are the ith EDR from OMI and ground observation, respectively.

To determine whether the calculated MB or NMB are statistically significant, a t-test for differences of mean under serial dependence is applied (Wilks, 2011). This two-sample t-test assumes a first-order autoregression in the data. The computed two-tailed p-value of less than 0.025 indicates that the difference between the means for the paired data (OMI and ground EDR) would be statistically significant at the 95% confidence level. In addition, we calculate the PDF and CDF of the OMI and ground observation. A Kolmogorov-Smirnov (K-S) test (Wilks, 2011) is performed to compare the CDFs of the OMI and ground datasets. The K-S test is represented by the following formula:

$$D = max\,|CDF_{OMI} - CDF_{Ground}|, \quad (4)$$

If D is greater than the critical value, $0.84\sqrt{1/n}$ (n is the total number of data points), then the null hypothesis that the two datasets were drawn from the same distribution will be rejected at the 99 % confidence level.

3.3 Trend analysis

Following the work of Weatherhead et al. (1997) and Weatherhead et al. (1998), the trend of surface UV irradiance from OMI and ground observation can be estimated using the following linear model:

$$Y_t = C + S_t + \omega X_t + N_t \qquad t = 1 \ldots T, \quad (5)$$

Where T is the total number of months considered and t is the month index, starting from January 2005 to December 2017. Y_t is the monthly mean surface UV irradiance either from OMI or the ground observation in the U.S. and C is a constant. X_t = t/12, represents the linear trend function and ω is the magnitude of the trend per year. S_t is a seasonal component, represented in the following form:

$$S_t = \sum_{j=1}^{4} [\beta_{1,j} \sin(2\pi jt/12) + \beta_{2,j} \cos(2\pi jt/12)], \quad (6)$$

N_t is the noise not represented by the linear model and is often assumed to be a first-order autoregressive model, which can be expressed as:

$$N_t = \phi N_{t-1} + \varepsilon_t, \quad (7)$$

Where N_{t-1} is the noise from month (t-1), ϕ is the autocorrelation between N_t and N_{t-1}, ε_t is the white noise which should be approximately independent, normally distributed with zero mean and common variance σ_ε^2.

As described in Weatherhead et al. (1998), General Least Squares (GLS) regression was applied to equation (5) to derive the approximation of ω and its standard deviation σ_ω as

$$\sigma_\omega = \frac{\sigma_N}{n^{3/2}} \sqrt{\frac{1+\phi}{1-\phi}}, \quad (8)$$

Where n = T/12, is the number of years of the data used in the analysis and σ_N is the standard deviation of N_t. We will consider the trend significant at the 95 % confidence level if $\omega/\sigma_\omega > 2$. Such linear models have been widely used to study the various environmental monthly time series data in the previous studies (Boys et al., 2014; Zhang and Reid, 2010; Weatherhead et al., 2000).

4 Results

4.1 Spatial and temporal inter-comparison

Figure 1 shows the map of OMI level 3 EDR at solar noon time under full-sky conditions averaged from 2005–2017, overlaid with 31 ground observational sites of EDR averaged from the same local noon time. First, we find that OMI data shows a meridional gradient with the dose rate increasing from ~ 80 mW m^{-2} in the northern U.S. to ~ 203 mW m^{-2} in the southern U.S. At higher elevation regions such as in Colorado, OMI-derived EDR are larger than other areas of the same latitude zone. In comparison, the ground sites range from ~ 71 mW m^{-2} in the northern U.S. to a maximum of ~ 200 mWm^{-2} for site NM01 in the southern U.S., generally capturing the OMI meridional gradient well. At most sites, OMI data overestimates the ground observation by more than 5 %, with sites in Steamboat Spring, Colorado (CO11), Burlington, Vermont (VT01) and Homestead, Florida (FL01) showing the highest bias of more than 15 %.

Scatter plots of OMI OP_FS and Noon_FS EDR with all 31 ground observational sites are shown in Fig. 2(a) and (b). In both cases, a linear relationship is found with correlation coefficient (R) of 0.88. This statistically significant correlation (with $P < 0.01$) can also be found at most individual sites, as shown in the Taylor Diagrams (Fig. 3(a) and (b)). The high correlation found here in the U.S. is consistent with previous work that evaluated OMI EDR in Europe (Buchard et al., 2008; Ialongo et al., 2008). However, lowest R of 0.66 and 0.65 at Florida (FL01) are found respectively for OMI OP_FS and Noon_FS EDR (shown in Fig. 2(c) and (d)). Even though both OMI OP_FS and Noon_FS EDR data show good correlation, their differences show different signs and magnitudes. Overall, we find that the MB for OMI OP_FS EDR comparison is –4.1 mW m^{-2} while the MB for OMI Noon_FS EDR comparison is 10.1 mW m^{-2}. The respect RMSE values are 39.8 and 42.2 mW m^{-2}. Figure 3 (a) and (b) show the evaluation of OMI OP_FS and Noon_FS EDR with D = 50 km and $\Delta T = \pm 5$ minutes for 31 ground observational sites in the form of a Taylor Diagram and Fig. 4(a) and (b) are the corresponding zoomed-in plots. As can be seen, with the case of OMI OP_FS EDR evaluation, 26 sites have negative NMB ranging from –14 % to –1.5 % with 16 sites being statistically significant at 95 % confidence level. Steamboat Springs, Colorado (CO11), Homestead, Florida (FL01) and Burlington, Vermont (VT01) show statistically significant (95 % confidence level) positive bias. The site in Holtville, California (CA21) shows no significant difference between OMI OP_FS EDR and ground observation. For OMI Noon_FS EDR, the majority of the sites have positive NMB (3–31 %) with site Steamboat Springs, Colorado (CO11) having the largest NMB of 31 %. The NMB found in most of the sites show significant difference at the 95 % confidence level except for sites in Holtville, California (CA21), Georgia (GA01) and Utah (UT01). With both datasets, the site at CO01 show high positive bias because of its high altitude (~ 3 km). The current OMI surface UV algorithm does not use any cloud correction for altitudes higher than 2.5 km, which leads to a clear-sky condition for higher altitudes.

The NSD of evaluating OMI OP_FS EDR for the majority of the sites varies from 0.75 to 1 (Fig. 4(a)), indicating that the OMI OP_FS EDR underestimates the amplitude of surface UV irradiance cycle found in the ground observation. In contrast, we find from Fig. 4(b) that about half of the ground sites have NSD values ranging from 1 to 1.1 while the rest of the sites have NSD values less than 1 for OMI Noon_FS EDR evaluation. In both cases, the ground site at Raleigh, North Carolina (NC01) has the lowest NSD of ~ 0.75. Additionally, sites in the southeastern U.S. (e.g., FL01, LA01, GA01, NC01) along with the site in Houston, Texas (TX41) all have relatively larger RMSD (greater than 0.5) for both OMI OP_FS and Noon_FS EDR evaluation according to Fig. 4(a) and (b), respectively. In comparison, sites in the northern higher latitude seem to show smaller RMSD (e.g., WA01, NE01, NY01, ND01). Overall, the site in Davis, California (CA01) show the best performance in terms of R, NSD and RMSD for both OMI OP_FS and Noon_FS EDR evaluation. These regional differences reflect the effects of the spatial variability of U.S. climate and air pollution on surface UV estimates. The southeastern U.S. is subject to heavy pollution and this region is largely affected by clouds. This could pose a greater challenge for the OMI surface UV algorithm. These discrepancies can be related to several factors such as the method of collocating OMI data with ground observation spatially and temporally, clouds in the atmosphere, and the assumption of constant atmospheric conditions between OMI overpass time and local solar noon time, which are discussed in the following sections.

To further show how well OMI surface EDR represents the ground observational EDR, the PDFs of both OMI and ground EDR are shown (Fig. 5). First, we find the distribution of surface EDR at solar noon time from both OMI and ground observational data show two peaks, one around 20 mW m^{-2} and the other one around 200 mW m^{-2}. Similar distribution with two peaks are also found for OMI and ground EDR at overpass time which are not shown here. These two peaks are largely due to the SZA effects, with the former one related to larger SZAs and the latter one with smaller SZAs. The work of Wang and Christopher (2006) also indicated that the change in SZA causes the solar downward shortwave irradiance to show two peaks one at ~08:00 LT and another one at ~16:00 LT. Figure 6 show the calculated CDFs for OMI and ground OP_FS and Noon_FS EDR as well as the maximum difference between EDRs at the corresponding time. The critical values for both comparisons are 0.087 to verify that the two CDFs show a good fit at the 99 % confidence level. From Fig. 6, we can see that both of the maximum differences are smaller than the critical values at the 99 % confidence level. Therefore, the null hypothesis (OMI surface EDR and ground observed EDR were drawn from the same distribution) will not be rejected. This good fit between OMI and ground EDR distribution for both solar noon time and overpass time again confirms the good correlation found between these two datasets.

In order to better understand the variability of surface UV, the peak UV frequency inferred from ground observation is investigated along with OMI Noon_FS EDR frequency. As seen in Fig. 7, both OMI Noon_FS and ground peak EDR show a high frequency at the lower end of surface EDR (< 100 mW m^{-2}), which also reflects the smaller peak found in Fig. 5. Moreover, this high frequency of occurrence persisted from 2005 to 2017 for both datasets. In addition, OMI Noon_FS EDR shows another high frequency of surface EDR around 200 mW m^{-2} corresponding to the other peak in Fig. 5. However, the ground peak does not capture this high frequency occurrence of ~ 200 mW m^{-2}, instead, the ground peak values find a high frequency around ~ 220 mW m^{-2} (shown in the red box in Fig. 7). This indicates that the OMI solar noon time EDR may not always represent the high peak value on a daily basis due to the varying atmospheric conditions. The high frequency occurrence of ~ 220 mW m^{-2} prevailed until 2015, at the same time, we find the frequency of higher surface EDR from ground peak of ~ 300 mW m^{-2} starts to increase around 2014 (shown in the red box in Fig. 7). This increase in the occurrence of peak UV intensity could have potential implications for human exposure and subsequent health effects, which is beyond the scope of this study.

4.2 Impacts of spatial collocation and temporal averaging

Table 4 and Table 5 summarize the regression statistics and other validation statistics of evaluating OMI OP_FS and Noon_FS EDR with different spatial collocation distances (D) and temporal averaging windows (ΔT), respectively. We find that the spatial collocation distances do not affect the overall comparison results significantly. Even though the stricter collocation distance within 10 km radius (or D = 10 km) results in 41 % decrease in MB for OMI OP_FS EDR evaluation, the collocated data sample size is reduced to only about 17 % of the original datasets. In contrast, the length of temporal averaging window seems to play a more important role in the overall comparison results. Figure 4 (a) to Figure 4(c) show that most of the dots representing the OMI OP_FS EDR evaluation on the Taylor Diagram are moving closer to the expected point as ΔT increases from ±5 minutes to ±60 minutes. The same progression is also found for OMI Noon_FS EDR evaluation which is not shown here. Specifically, the increasing temporal windows cause the NSD values to increase. On the other hand, R increases and RMSD decreases as temporal average window ΔT increases from ±5 minutes to ±60 minutes in both cases, which can be also found in Fig. 4(d). Moreover, the RMSE values decrease by about 16.8 % and 11.1 % as ΔT increase from ±5 minutes to ±60 minutes for OP_FS and Noon_FS EDR comparison, respectively. The improvement with a longer temporal averaging window for overpass time under full-sky is also found by Zempila et al. (2016). Additionally, changes in the sign of NMB from negative to positive are found at some of the sites for OMI OP_FS evaluation when ΔT increases from ±5 minutes to ±60 minutes. The positive NMB is significant for sites CA21, TX41, MS01, ME01, MT01 and VT01. This could suggest that atmospheric conditions do not stay the same over this longer temporal averaging window.

4.3 Impacts of the assumption of constant atmospheric conditions

As described in Sect. 2.1, the current surface UV algorithm assumes the same atmospheric conditions at OMI overpass time and the local solar noon time regarding cloudiness, total column ozone and atmospheric aerosol loadings but with different SZAs. However, this assumption may not hold all the time for the real atmosphere. We take the ratio between Noon_FS and OP_FS EDR (Noon_FS/OP_FS) from both OMI and ground data as an indicator of the variation of atmospheric conditions between these two times. Figure 8 shows the frequency and PDF of this ratio from both OMI and ground data obtained with

D = 50 km and ΔT = ±5 minutes. The ground ratio is approximately equally distributed around the center of 1 while about 95 % of the OMI data falls into the area with the ratio greater than 1. This indicates that the current OMI surface UV algorithm would not fully represent the real atmosphere with the assumption of constant atmospheric conditions being made and could thus induce errors in estimating surface UV irradiances. The scatter plot of the ground ratio and OMI ratio further confirms the inconsistency between the OMI data and the observational data (Fig. 9) with no significant correlation being found.

We further investigate the possible seasonal effects on this ratio. As can be seen in Fig. 10, the mean and median ratio (Noon_FS/OP_FS) from OMI are greater than those from the ground observational data throughout the year, which again indicates the potential overestimation of OMI Noon_FS EDR using constant atmospheric conditions. Furthermore, the discrepancy between these two ratios stays consistent in the spring and summer time. The smaller SZA in the summer time would have relatively small effects and the difference in these ratios could be largely affected by the varying atmospheric conditions between local solar noon time and OMI overpass time. However, this discrepancy becomes larger in the fall and winter time, which could be the result of the elevated SZA towards winter time in North America to some extent. The larger SZA (> 70º) in the colder times could increase the radiation path in the atmosphere which would thereby amplify the atmospheric interaction with the solar radiation. Besides, other seasonal variables such as the climatological albedo used in the current OMI surface UV algorithm could potentially play a role in the deviation between OMI and ground data. In addition, the ratio from both OMI and ground observational data show larger variation in the fall and winter season than its respective summer season, implying the impacts of the SZA seasonal variation on both OMI and observational data.

The SZA seasonal variation could subsequently affect the difference between OMI and ground data, which will be analyzed in this section. Several previous studies have investigated the effects of SZA on the difference between OMI and ground observational irradiance. Buchard et al. (2008) found that OMI spectral UV irradiance on clear-sky days showed a larger discrepancy at SZA greater than 65º. Kazadzis et al. (2009) found no systematic dependence of the difference between OMI and ground observational spectral UV irradiance on SZA. By sorting data based on cloud and aerosol conditions, Antón et al. (2010) showed that the relative difference between OMI and ground irradiance decreases modestly with SZA for all-sky conditions except for days with high aerosol loadings. Zempila et al. (2016) suggested a small dependence of the ratio (OMI/ground UV irradiance) on SZA under both clear-sky and all-sky conditions. For the all-sky condition, the ratio increases steadily with increasing SZA up to 50º and becomes larger than one after 50º. From the simple regression derived using bin averaged data (Fig. 11), we find that the OMI OP_FS EDR bias has a stronger dependence on the overpass SZA than Noon_FS EDR. At smaller SZAs, the median of OMI OP_FS EDR bias show smaller dependence, however, the median increases greatly (up to –30%) when SZA is greater than ~ 65 º.

Clouds also play an important role in the difference between OMI and ground observational UV irradiance. Buchard et al. (2008) found that the relative difference between OMI and ground EDR was associated with COT at 360 nm retrieved from

OMI and the difference is more appreciable for large COT. Tanskanen et al. (2007) showed that the distribution of the OMI and ground EDD ratio widens with increasing COT. Antón et al. (2010) used OMI retrieved LER at 360 nm as a proxy for cloudiness and showed that the relative difference of OMI and ground EDR increased largely at higher LER values. Here, we find that the relative bias for OMI OP_FS EDR is more obvious at larger COT values as well (Fig. 12). In addition, the noise of the bias gets larger at higher COT values. This is due to the fact that OMI surface UV algorithm uses the average of a pixel to represent the cloudiness in that specific pixel. In reality, the spatial distribution of cloudiness in that pixel could vary a lot which could result in the large difference in surface UV irradiance between the OMI pixel and the ground observational site.

4.4 Trend analysis

EDR is the weighted solar irradiance from 300–400 nm which covers the UVB range principally controlled by the atmospheric ozone column. In addition, both UVA and UVB could be affected by the cloud cover and aerosol loadings in the atmosphere. Thus, the identified trend of surface EDR could be a result of the combined effects of the aforementioned different factors and it would be challenging to attribute the trend to any individual factor quantitatively. Therefore, we focus on providing a descriptive summary of surface EDR trends derived from both OMI and ground observation.

We first analyze the surface EDR trend using OMI level 3 data. We find that OMI full-sky solar noon EDR data show a positive trend in most of the places; but the only significant trend (95 % confidence level) was found in parts of the northeastern U.S., in parts of the Ohio River valley region and in a small part of California (Fig. 13(b)). A similar distribution of trend is found in OMI level 3 full-sky spectral irradiance at 310 nm (Fig. 14 (a)). We also analyzed the trend of OMI level 3 clear-sky EDR and total column ozone amount (not shown here) and found no significant trend in either dataset. This could suggest that the contribution of ozone column to the estimated trend of OMI full-sky EDR is minimal. Instead, the estimated trend could be induced by other factors such as changes in the local cloudiness and absorbing aerosols. No significant trends of OMI AOD and COT are found over U.S. in this work. Zhang et al. (2017) found significant positive trends over the western U.S. using OMI AOD for 2005–2015 and Hammer et al. (2018) found small positive trends over the western and central U.S. with OMI AOD (388 nm) from the OMI OMAERUV algorithm for 2005–2015. However, we find significant positive trends of OMI AAOD at 388 nm in part of the central and eastern U.S. and western U.S. close to the coast (Fig. 14(b)). Zhang et al. (2017) found a significant increase in OMI AAOD in the southern and central U.S. and proposed that this increase is largely caused by dust AAOD. The OMI surface UV algorithm uses a monthly mean climatological aerosol data (Kinne, 2009), and it may not be well updated to represent the role of absorbing aerosols in attenuating the surface UV radiation considering the diurnal and day to day variations, which may result in the contrasting trends of OMI AAOD and surface EDR in the northeastern U.S. and the Ohio River Valley region found here.

In contrast, ground observation shows different trend patterns using two different sampling methods. For both methods, only months with more than 10 days of data are used for trend analysis and considered missing values otherwise. The first method is to average the ground observational data with D = 50 km and ΔT = ±5 minutes around local solar noon time, denoted as once-per-day sampling. Eighteen of 31 sites are found to have significant trends at the 95 % confidence level (Fig. 13 (b)). Seven sites have positive trends while the rest of the 11 sites show negative trends. The second method averages all the data in a day at each site, hereby referred to as all-per-day sampling. We find that this method results in 15 sites with significant trends at the 95% confidence level (Fig 13(c)). Only 4 of the 15 sites have positive trends with the rest of the sites showing negative trends.

Both methods (e.g., once-per-day and all-per-day) find significant negative trends for sites in the Northeast and the Ohio River Valley region with all-per-day method showing smaller trends. Using the site IN01 as an example, Figure 15 illustrates the difference between these two sampling methods. Both methods could capture the seasonal variation of the surface EDR, however, the magnitude of all-per-day sampling EDR is about 3 times smaller than that of the once-per-day sampling, which is anticipated because the all-per-day average is smaller than one-per-day measurement around noon time. By averaging all the daytime data, the all-per-day sampling method smooths out the atmospheric conditions throughout the day. In contrast, the estimated trend of OMI Noon_FS EDR at this site is not significant, and this contrast suggests the importance to account for the variation of atmospheric conditions throughout the daytime. The estimated positive trend from OMI AAOD at this region could be the cause of the negative trend derived from the observed EDR, further suggesting the need to consider the change of AAOD in estimating surface UV radiation.

5 Conclusion and discussion

In this study, we evaluated the OMI surface erythemal irradiance at overpass time and solar noon time for the period of 2005–2017 with 31 UVMRP ground sites in the continental United States. The OMI surface Noon_FS EDR shows a meridional gradient with the EDR increasing from ~ 80 mW m^{-2} in the northern U.S. to ~ 203 mW m^{-2} in the southern U.S. The ground observational data could capture this gradient well with EDR increasing from ~ 71 mW m^{-2} in the northern U.S. to maximum of ~ 200 mW m^{-2} in the southern sites.

The comparison for both OMI OP_FS and Noon_FS EDR show good correlation with the counterparts from ground-based measurements, with R = 0.88 when the data is matched with D = 50 km and ΔT = ±5 minutes. However, the bias differs in signs and magnitudes. Overall, the OMI OP_FS EDR underestimates the ground observational data by –4.1 mW m^{-2} while OMI Noon_FS EDR overestimates by 10.1 mW m^{-2}. The RMSEs are 39.8 and 42.2 mW m^{-2} respectively. The biases also show large spatial variability. For OMI OP_FS EDR, the NMB ranges from –14 % to –1.5 % for most sites while several sites (FL01, VT01 and CO11) show positive biases. In comparison, most sites for OMI Noon_FS EDR evaluation show positive NMB ranging from 3 % to 31 %. Furthermore, for both OMI OP_FS and Noon_FS EDR comparison, R increases as the temporal averaging windows ΔT increases from ±5, ±10, ±30, to ±60 minutes. When the temporal average window reaches ±60 minutes, the OMI OP_FS EDR bias changes from negative to positive for some sites. This suggests that the atmospheric condition does not stay consistent even within an hour, underscoring the importance of geostationary satellite measurements. The relatively large bias and RMSE in magnitude for OMI Noon_FS EDR suggests the importance to account for the variation of atmospheric conditions between solar noon and satellite overpass time, which cannot be resolved by polar-orbiting satellite measurements but future geostationary satellites such as TEMPO, Sentinel-4 and GEMS should be able to resolve this issue.

We also extended the evaluation of OMI and ground EDR by comparing the PDFs and CDFs as well as considering the peak UV variability. First, both OMI and ground EDR distributions show two peaks, one around 20 and another around 200 mW m^{-2}, mainly related to larger and smaller SZAs, respectively. The K-S test shows that the OMI and ground EDR are from the same sample distribution at the 99 % confidence level. Both OMI Noon_FS and ground peak EDR show the high frequency occurrence of the smaller peak (~ 20 mW m^{-2}) over the period of 2005–2017. However, the other high frequency occurrence of OMI Noon_FS EDR (~ 200 mW m^{-2}) is not consistent with the high frequency found in ground peak values (~ 220 mW m^{-2}), which again reveals that the OMI solar noon time may not always capture the peak UV values in a day, thus highlighting the necessity for finer temporal resolution data.

Ground-based continuous measurements were used to show the effects of atmospheric variation on surface EDR. The ratio of OMI Noon_FS / OP_FS EDR is greater than 1 for 95 % of the data points, while the ratio derived from the ground-based data has a Gaussian distribution centered around 1. This means that the assumption of a consistent cloudiness, column ozone amount and aerosol loadings between these two times would lead to large positive bias in the estimates of surface UV at solar noon time, which is revealed in this study. Furthermore, we find that the OMI OP_FS EDR bias show some negative dependence on the SZAs. Overall, the bias is smaller at smaller SZAs but increases greatly up to –30% when the SZA is greater than ~ 65°. Additionally, the OMI OP_FS EDR bias shows slight dependence on COT. The error distribution of the bias gets much wider at larger COT values. This error statistics suggests the importance of multiple scattering by aerosols and clouds in the radiative transfer model, which is overlooked in the radiative transfer calculation for the current OMI's look-up table approach to estimate surface UV.

Lastly, we investigated the surface UV trend from both OMI and ground observational data. Significant positive trends were found in parts of the northeastern U.S., in the Ohio River Valley region and in a small part of California from OMI full-sky data during solar noon time. In contrast, the trend from ground data depends on sampling method. The once-per-day sampling at noon time shows larger spatial variability in the magnitude and signs of the trend while the all-per-day sampling shows less variation in the magnitude. The all-per-day sampling method would smooth the variation in the surface UV data that may result in a more uniform trend compared with the once-per-day sampling. The difference in the estimated trends from these two methods is greater for sites in the western and central U.S. Analysis using ground-based observation with two methods and OMI data reveal contrasting trend in the Northeast and in the Ohio River valley, implying the climatological AAOD may not well account for the day to day and diurnal variations. While no discernable column ozone and COT trend from OMI are found, decreasing trends of surface UV, as revealed by both methods using ground-based data, seem to be consistent with the increasing trend of OMI AAOD, further suggesting the need to consider AAOD variability in estimates of surface UV.

Acknowledgements

The research was funded by NASA's Aura satellite program (managed by Dr. Kenneth W. Jucks), Applied Sciences program (managed by John A. Haynes), and Atmospheric Composition and Analysis Program (ACMAP managed by Dr. Richard Eckman). The authors thank the OMI team for providing the surface UV and aerosol products, which can be downloaded from the NASA Goddard Earth Sciences (GES) Data and Information Services Center (DISC) (https://disc.gsfc.nasa.gov). We also thank the UVMRP for the ground observational UV data, which is available at https://uvb.nrel.colostate.edu/UVB/uvb-dataAccess.jsf.

References

Antón, M., Cachorro, V., Vilaplana, J., Toledano, C., Krotkov, N., Arola, A., Serrano, A., and Morena, B.: Comparison of UV irradiances from Aura/Ozone Monitoring Instrument (OMI) with Brewer measurements at El Arenosillo (Spain)–Part 1: Analysis of parameter influence, Atmospheric Chemistry and Physics, 10, 5979-5989, 2010.

Arola, A., Kazadzis, S., Krotkov, N., Bais, A., Gröbner, J., and Herman, J. R.: Assessment of TOMS UV bias due to absorbing aerosols, Journal of Geophysical Research: Atmospheres, 110, 2005.

Arola, A., Kazadzis, S., Lindfors, A., Krotkov, N., Kujanpää, J., Tamminen, J., Bais, A., di Sarra, A., Villaplana, J. M., Brogniez, C., Siani, A. M., Janouch, M., Weihs, P., Webb, A., Koskela, T., Kouremeti, N., Meloni, D., Buchard, V., Auriol, F., Ialongo, I., Staneck, M., Simic, S., Smedley, A., and Kinne, S.: A new approach to correct for absorbing aerosols in OMI UV, Geophysical Research Letters, 36, 10.1029/2009GL041137, 2009.

Bernhard, G., and Seckmeyer, G.: Uncertainty of measurements of spectral solar UV irradiance, Journal of Geophysical Research: Atmospheres, 104, 14321-14345, 1999.

Bernhard, G., Arola, A., Dahlback, A., Fioletov, V., Heikkilä, A., Johnsen, B., Koskela, T., Lakkala, K., Svendby, T., and Tamminen, J.: Comparison of OMI UV observations with ground-based measurements at high northern latitudes, Atmospheric Chemistry and Physics, 15, 7391-7412, 2015.

Bigelow, D. S., Slusser, J., Beaubien, A., and Gibson, J.: The USDA ultraviolet radiation monitoring program, Bulletin of the American Meteorological Society, 79, 601-615, 1998.

Bornman, J. F., and Teramura, A. H.: Effects of ultraviolet-B radiation on terrestrial plants, in: Environmental UV photobiology, Springer, 427-471, 1993.

Boys, B., Martin, R., Van Donkelaar, A., MacDonell, R., Hsu, N., Cooper, M., Yantosca, R., Lu, Z., Streets, D., and Zhang, Q.: Fifteen-year global time series of satellite-derived fine particulate matter, Environmental science & technology, 48, 11109-11118, 2014.

Buchard, V., Brogniez, C., Auriol, F., Bonnel, B., Lenoble, J., Tanskanen, A., Bojkov, B., and Veefkind, P.: Comparison of OMI ozone and UV irradiance data with ground-based measurements at two French sites, Atmospheric Chemistry and Physics, 8, 4517-4528, 2008.
Caldwell, M., Teramura, A. H., Tevini, M., Bornman, J., Björn, L. O., and Kulandaivelu, G.: Effects of increased solar ultraviolet-radiation on terrestrial plants, Ambio, 24, 166-173, 1995.
Cede, A., Luccini, E., Nuñez, L., Piacentini, R. D., Blumthaler, M., and Herman, J. R.: TOMS-derived erythemal irradiance versus measurements at the stations of the Argentine UV Monitoring Network, Journal of Geophysical Research: Atmospheres, 109, 2004.
Chubarova, N. Y., Yurova, A. Y., Krotkov, N. A., Herman, J. R., and Bhartia, P. K.: Comparisons between ground measurements of UV irradiance 290 to 380nm and TOMS UV estimates over Moscow for 1979-2000, Opt. Eng. 0001 41 (12), 3070-3081, 2002.
Deirmendjian, D.: Electromagnetic scattering on spherical polydispersions, RAND CORP SANTA MONICA CA, 1969.
Eck, T. F., Bhartia, P. K., and Kerr, J. B.: Satellite estimation of spectral UVB irradiance using TOMS derived total ozone and UV reflectivity, Geophysical Research Letters, 22, 611-614, 10.1029/95GL00111, 1995.
Eide, M. J., and Weinstock, M. A.: Association of UV index, latitude, and melanoma incidence in nonwhite populations—US Surveillance, Epidemiology, and End Results (SEER) Program, 1992 to 2001, Archives of dermatology, 141, 477-481, 2005.
Farman, J. C., Gardiner, B. G., and Shanklin, J. D.: Large losses of total ozone in Antarctica reveal seasonal ClOx/NOx interaction, Nature, 315, 207, 1985.
Fioletov, V., Bodeker, G., Miller, A., McPeters, R., and Stolarski, R.: Global and zonal total ozone variations estimated from ground-based and satellite measurements: 1964–2000, Journal of Geophysical Research: Atmospheres, 107, 2002.
Hammer, M. S., Martin, R. V., Li, C., Torres, O., Manning, M., and Boys, B. L.: Insight into global trends in aerosol composition from 2005 to 2015 inferred from the OMI Ultraviolet Aerosol Index, Atmospheric Chemistry and Physics, 18, 8097-8112, 2018.
Herman, J., Krotkov, N., Celarier, E., Larko, D., and Labow, G.: Distribution of UV radiation at the Earth's surface from TOMS-measured UV-backscattered radiances, Journal of Geophysical Research: Atmospheres, 104, 12059-12076, 1999.
Ialongo, I., Casale, G., and Siani, A.: Comparison of total ozone and erythemal UV data from OMI with ground-based measurements at Rome station, Atmospheric Chemistry and Physics, 8, 3283-3289, 2008.
Janjai, S., Wisitsirikun, S., Buntoung, S., Pattarapanitchai, S., Wattan, R., Masiri, I., and Bhattarai, B.: Comparison of UV index from Ozone Monitoring Instrument (OMI) with multi-channel filter radiometers at four sites in the tropics: effects of aerosols and clouds, International Journal of Climatology, 34, 453-461, 2014.
Kalliskota, S., Kaurola, J., Taalas, P., Herman, J. R., Celarier, E. A., and Krotkov, N. A.: Comparison of daily UV doses estimated from Nimbus 7/TOMS measurements and ground-based spectroradiometric data, Journal of Geophysical Research: Atmospheres, 105, 5059-5067, 2000.
Kazadzis, S., Bais, A., Arola, A., Krotkov, N., Kouremeti, N., and Meleti, C.: Ozone Monitoring Instrument spectral UV irradiance products: comparison with ground based measurements at an urban environment, Atmospheric Chemistry and Physics, 9, 585-594, 2009.
Kazantzidis, A., Bais, A., Gröbner, J., Herman, J., Kazadzis, S., Krotkov, N., Kyrö, E., Den Outer, P., Garane, K., and Görts, P.: Comparison of satellite-derived UV irradiances with ground-based measurements at four European stations, Journal of Geophysical Research: Atmospheres, 111, 2006.
Kinne, S.: Climatologies of cloud-related aerosols. Part 1: Particle number and size, in: Clouds in the perturbed climate system, MIT Press, 37-57, 2009.
Koh, H. K., Geller, A. C., Miller, D. R., Grossbart, T. A., and Lew, R. A.: Prevention and early detection strategies for melanoma and skin cancer: current status, Archives of dermatology, 132, 436-443, 1996.
Krotkov, N. A., Bhartia, P. K., Herman, J. R., Fioletov, V., and Kerr, J.: Satellite estimation of spectral surface UV irradiance in the presence of tropospheric aerosols: 1. Cloud-free case, Journal of Geophysical Research: Atmospheres, 103, 8779-8793, 10.1029/98JD00233, 1998.
Krotkov, N. A., Herman, J. R., Bhartia, P. K., Fioletov, V., and Ahmad, Z.: Satellite estimation of spectral surface UV irradiance: 2. Effects of homogeneous clouds and snow, Journal of Geophysical Research: Atmospheres, 106, 11743-11759, 10.1029/2000JD900721, 2001.

Krotkov, N. A., Herman, J., Bhartia, P., Seftor, C., Arola, A., Kaurola, J., Taalas, P., and Vasilkov, A.: OMI surface UV irradiance algorithm, Algorithm Theoretical Baseline Document: Clouds, Aerosols, and Surface UV Irradiance, 3, 2002.

Lantz, K. O., Disterhoft, P., DeLuisi, J. J., Early, E., Thompson, A., Bigelow, D., and Slusser, J.: Methodology for deriving clear-sky erythemal calibration factors for UV broadband radiometers of the US Central UV Calibration Facility, Journal of Atmospheric and Oceanic Technology, 16, 1736-1752, 1999.

Lemus-Deschamps, L., and Makin, J. K.: Fifty years of changes in UV Index and implications for skin cancer in Australia, International journal of biometeorology, 56, 727-735, 2012.

Levelt, P. F., van den Oord, G. H., Dobber, M. R., Malkki, A., Visser, H., de Vries, J., Stammes, P., Lundell, J. O., and Saari, H.: The ozone monitoring instrument, IEEE Transactions on geoscience and remote sensing, 44, 1093-1101, 2006.

McKenzie, R., Seckmeyer, G., Bais, A., Kerr, J., and Madronich, S.: Satellite retrievals of erythemal UV dose compared with ground-based measurements at northern and southern midlatitudes, Journal of Geophysical Research: Atmospheres, 106, 24051-24062, 2001.

McKenzie, R., Smale, D., and Kotkamp, M.: Relationship between UVB and erythemally weighted radiation, Photochemical & Photobiological Sciences, 3, 252-256, 2004.

McKenzie, R., Bodeker, G., Scott, G., Slusser, J., and Lantz, K.: Geographical differences in erythemally-weighted UV measured at mid-latitude USDA sites, Photochemical & Photobiological Sciences, 5, 343-352, 2006.

McKinlay, A., and Diffey, B.: A reference action spectrum for ultraviolet erythema in human skin, CIE journal, 6, 17-22, 1987.

Sabburg, J., Rives, J., Meltzer, R., Taylor, T., Schmalzle, G., Zheng, S., Huang, N., Wilson, A., and Udelhofen, P.: Comparisons of corrected daily integrated erythemal UVR data from the US EPA/UGA network of Brewer spectroradiometers with model and TOMS-inferred data, Journal of Geophysical Research: Atmospheres, 107, 2002.

Scotto, J., Cotton, G., Urbach, F., Berger, D., and Fears, T.: Biologically effective ultraviolet radiation: surface measurements in the United States, 1974 to 1985, Science, 239, 762-764, 1988.

Tanskanen, A., Krotkov, N. A., Herman, J. R., and Arola, A.: Surface ultraviolet irradiance from OMI, IEEE transactions on Geoscience and Remote Sensing, 44, 1267-1271, 2006.

Tanskanen, A., Lindfors, A., Määttä, A., Krotkov, N., Herman, J., Kaurola, J., Koskela, T., Lakkala, K., Fioletov, V., and Bernhard, G.: Validation of daily erythemal doses from Ozone Monitoring Instrument with ground-based UV measurement data, Journal of Geophysical Research: Atmospheres, 112, 2007.

Taylor, K. E.: Summarizing multiple aspects of model performance in a single diagram, Journal of Geophysical Research: Atmospheres, 106, 7183-7192, 2001.

Torres, O., Tanskanen, A., Veihelmann, B., Ahn, C., Braak, R., Bhartia, P. K., Veefkind, P., and Levelt, P.: Aerosols and surface UV products from Ozone Monitoring Instrument observations: An overview, Journal of Geophysical Research: Atmospheres, 112, 2007.

UNEP: Environmental effects of ozone depletion and its interactions with climate change: 2006 assessment, Photochemical & Photobiological Sciences, 6, 201-332, 10.1039/b700016b, 2007.

Walls, A. C., Han, J., Li, T., and Qureshi, A. A.: Host risk factors, ultraviolet index of residence, and incident malignant melanoma in situ among US women and men, American journal of epidemiology, 177, 997-1005, 2013.

Wang, J., and Christopher, S. A.: Mesoscale modeling of Central American smoke transport to the United States: 2. Smoke radiative impact on regional surface energy budget and boundary layer evolution, Journal of Geophysical Research: Atmospheres, 111, 2006.

Weatherhead, E. C., Tiao, G. C., Reinsel, G. C., Frederick, J. E., DeLuisi, J. J., Choi, D., and Tam, W. k.: Analysis of long-term behavior of ultraviolet radiation measured by Robertson-Berger meters at 14 sites in the United States, Journal of Geophysical Research: Atmospheres, 102, 8737-8754, 1997.

Weatherhead, E. C., Reinsel, G. C., Tiao, G. C., Meng, X. L., Choi, D., Cheang, W. K., Keller, T., DeLuisi, J., Wuebbles, D. J., and Kerr, J. B.: Factors affecting the detection of trends: Statistical considerations and applications to environmental data, Journal of Geophysical Research: Atmospheres, 103, 17149-17161, 1998.

Weatherhead, E. C., Reinsel, G. C., Tiao, G. C., Jackman, C. H., Bishop, L., Frith, S. M. H., DeLuisi, J., Keller, T., Oltmans, S. J., and Fleming, E. L.: Detecting the recovery of total column ozone, Journal of Geophysical Research: Atmospheres, 105, 22201-22210, 2000.

Weihs, P., Blumthaler, M., Rieder, H., Kreuter, A., Simic, S., Laube, W., Schmalwieser, A., Wagner, J., and Tanskanen, A.: Measurements of UV irradiance within the area of one satellite pixel, Atmospheric Chemistry and Physics, 8, 5615-5626, 2008.

Wilks, D. S.: Chapter 5 - Frequentist Statistical Inference, in: International Geophysics, edited by: Wilks, D. S., Academic Press, 133-186, 2011.

WMO: Global UV Index: A Practical Guide. , WHO/SDE/OEH/02.2, Geneva, Switzerland, 2002.

WMO: Scientific Assessment of Ozone Depletion:2010, Global Ozone Research and Monitoring Project-Report NO.52, 516pp., Geneva, Switzerland,2011, 2010.

Zempila, M.-M., Koukouli, M.-E., Bais, A., Fountoulakis, I., Arola, A., Kouremeti, N., and Balis, D.: OMI/Aura UV product validation using NILU-UV ground-based measurements in Thessaloniki, Greece, Atmospheric Environment, 140, 283-297, 2016.

Zhang, J., and Reid, J.: A decadal regional and global trend analysis of the aerosol optical depth using a data-assimilation grade over-water MODIS and Level 2 MISR aerosol products, Atmospheric Chemistry and Physics, 10, 10949-10963, 2010.

Zhang, L., Henze, D. K., Grell, G. A., Torres, O., Jethva, H., and Lamsal, L. N.: What factors control the trend of increasing AAOD over the United States in the last decade?, Journal of Geophysical Research: Atmospheres, 122, 1797-1810, 2017.

Atmos. Chem. Phys. Discuss., https://doi.org/10.5194/acp-2018-720
Manuscript under review for journal Atmos. Chem. Phys.
Discussion started: 3 September 2018

Table 1. Summary of previous studies evaluating OMI surface UV data against ground observation. Most of the comparisons shown here are for all-sky conditions unless noted otherwise.

Study	Location	OMI data[a]	Ground instrument	Time periods	Bias[b]
(Kazadzis et al. 2009)	Thessaloniki, Greece	Spectral (op)	Brewer MK III	Sep 2004–Dec 2007	30 % (305 nm), 17 % (324 nm), 13 % (380 nm)[c]
(Antón et al. 2010)	El Arenosillo, Spain	Spectral (op)	Brewer MK III	Oct 2004–Dec 2008	14.2 % (305 nm), 10.6 % (310 nm), 8.7 % (324 nm)[d]
		EDR (op)			12.3 %
(Zempila et al. 2016)	Thessaloniki, Greece	Spectral (op)	NILU-UV multi-filter radiometer	Jan 2005–Dec 2014	31 % (305 nm), 29.5 % (310 nm), 6.1 % (324 nm), 14.0 % (380 nm)[e]
		Spectral (noon)			33.6 % (305 nm), 28.6 % (310 nm), 5.6 % (324 nm), 13.2 % (380 nm)
(Buchard et al. 2008)	Villeneuve d' Ascq, France	EDR (op)	spectroradiometer[f]	Oct 2005–Feb 2007	32.5 %[h]
			UVB-1, YES[g]		69.3 %
		EDD	spectroradiometer	Oct 2005–Jul 2006	17.1 %
	Briançon, France	EDD	spectroradiometer	Oct 2004–Sep 2005	7.9 %
(Ialongo, Casale, and Siani 2008)	Rome, Italy	EDR (noon)	Brewer MKIV	Sep 2004–Jul 2006	33 %[i]
			UVB-1, YES		30 %
(Tanskanen et al. 2007)[j]	17 sites	EDD	18 instruments	Sep 2004–Mar 2006	up to 50 %[k]
(Bernhard et al. 2015)[l]	13 stations	EDD	13 instruments	Sep 2004–Dec 2012	–1 % to 24 %[m]
(Weihs et al. 2008)[n]	Vienna, Austria	UV index (op)	Biometer	May–Jul 2007	–10 % to 50 %[o]
(Janjai et al. 2014)[p]	Thailand	UV index (op)	Multi-channel UV radiometer	2008–2010	43.6 %, 43.5 %, 28.7 %, 21.9 %[q]

[a]Spectral represents the OMI spectral irradiance data, EDR is the erythemal dose rate and EDD is the erythemally weighted daily dose. Op corresponds to the OMI data at its overpass time while noon means the data at local solar noon time.

[b]The validation statistic shown here is the bias with each study using slight different ways of calculation.

[c]The bias here is calculated as the median (OMI/Ground – 1) * 100.

[d]The bias is calculated as $100 \cdot \frac{1}{N}\sum_{i=1}^{N}\frac{OMI-Ground}{OMI}$, where N is the total number of data points.

[e]The bias is calculated as the mean (OMI – Ground)/Ground *100.

[f]The spectroradiometer used here is thermally regulated Jobin Yvon H10 double monochromators.

[g]The broadband UVB-1 is from Yankee Environmental System (YES).

[h]The bias is calculated as $100 \cdot \frac{1}{N}\sum_{i=1}^{N}\frac{OMI-Ground}{Ground}$, where N is the total number of data points.

[i]Same as [h].

[j]This study evaluated OMI surface EDD at 17 ground sites representing different latitudes, elevations and climate conditions with 18 instruments, which include single and double Brewer spectrophotometers, NIWA UV Spectrometer Systems, DILOR XY50 spectrometer, and SUV spectroradiometers. More detailed information can be found in this study.

[k]The bias is calculated same as [c]. For sites significantly affected by absorbing aerosols or trace gases, the bias can be up to 50 %.

[l]This study evaluated OMI EDD at 13 ground stations located throughout the Arctic and Scandinavia from 60° to 83º N. The instruments installed include single-monochromator Brewer spectrophotometer, GUV-541 and GUV-511 multi-filter radiometers from Biospherical Instrument Inc. (BSI).

[m]Same as [c].

[n]This study evaluated OMI UV index at 6 ground stations in the city of Vienna, Austria, and its surroundings. 6 Biometers (Model 501, Solar Light) were used.

[o]The bias is calculated as (OMI/Ground – 1) * 100 and here shown is the result for clear-sky conditions.

[p]This study evaluated OMI UV index at four tropical sites in Thailand with each site having different time periods of data between 2008–2010. The ground instrument installed is a multi-channel UV radiometer (GUV-2511) manufactured by BSI.

[q]The bias is calculated as [h], representing the four sites, respectively.

1 **Table 2. OMI data products and validation statistics used in the current study.**

	Full name	Acronym	Unit
Data products	Full-sky overpass time erythemal dose rate	OP_FS EDR	mW m^{-2}
	Full-sky solar noon erythemal dose rate	Noon_FS EDR	mW m^{-2}
Validation statistics	Mean bias	MB	mW m^{-2}
	Normalized mean bias	NMB	%
	Root-mean-square error	RMSE	mW m^{-2}
	Root-mean-square difference	RMSD	mW m^{-2}
	Normalized standard deviation	NSD	unitless

2

3

1 **Table 3. The 31 ground observational sites from UVMRP and their geographical information.**

Station ID	Location	Latitude (°N)	Longitude (°W)	Elevation (m)
AZ01	Flagstaff, AZ	36.06	112.18	2073
CA01	Davis, CA	38.53	121.78	18
CA21	Holtville, CA	32.81	115.45	-18
CO01	Nunn, CO	40.81	104.76	1641
CO11	Steamboat Springs, CO	40.46	106.74	3220
CO41	Lamar, CO	38.07	102.62	1131
FL01	Homestead, FL	25.39	80.68	0
GA01	Griffin, GA	33.18	84.41	267
IL01	Bondville, IL	40.05	88.37	213
IN01	West Lafayette, IN	40.47	86.99	216
LA01	Baton Rouge, LA	30.36	91.17	6
MD01	Queenstown, MD	38.92	76.15	5
MD11	Beltsville, MD	39.01	76.95	64
ME11	Presque Isle, ME	46.70	68.04	155
MI01	Pellston, MI	45.56	84.68	230
MN01	Grand Rapids, MN	47.18	93.53	424
MT01	Poplar, MT	48.31	105.10	634
MS01	Starkville, MS	33.47	88.78	88
NC01	Raleigh, NC	35.73	78.68	120
ND01	Fargo, ND	46.90	96.81	275
NE01	Mead, NE	41.15	96.49	355
NM01	Las Cruces, NM	32.62	106.74	1317
NY01	Geneva, NY	42.88	77.03	219
OK01	Billings, OK	36.60	97.49	317
ON01	Toronto, ON	43.78	79.47	210
TX21	Seguin, TX	29.57	97.98	172
TX41	Houston, TX	29.72	95.34	76
UT01	Logan, UT	41.67	111.89	1369
VT01	Burlington, VT	44.53	72.87	390
WA01	Pullman, WA	46.76	117.19	805

WI01	Dancy, WI	44.71	89.77	381

Atmos. Chem. Phys. Discuss., https://doi.org/10.5194/acp-2018-720
Manuscript under review for journal Atmos. Chem. Phys.
Discussion started: 3 September 2018

Table 4. Regression statistics and other validation statistics for evaluating OMI OP_FS EDR with 31 ground observational sites using different spatial collocation distances and temporal averaging windows.

statistics[a]	D = 50[b]				D = 25	D = 10
	5 min[c]	10 min	30 min	60 min	5 min	5 min
N	100801	100824	100880	100938	67628	17479
R	0.88	0.88	0.90	0.91	0.87	0.87
Slope	0.8	0.82	0.85	0.88	0.81	0.83
Intercept	19.8	18.1	15.2	13.1	19.7	18.7
MB	-4.1	-4.0	-3.4	-1.1	-3.7	-2.4
RMSE	39.8	38.4	35.6	33.1	40.7	40.5

[a]N is the total number of data pairs between OMI and ground observation for 31 sites altogether. R, slope, and intercept are the values obtained from the linear regression. MB and RMSE represent the mean bias and root-mean-square error as calculated in Eq. (1) and (2), respectively.

[b]D = 50, 25, 10 are the spatial collocation distances (D = 50 km, 25 km, 10 km) between an OMI ground pixel center and a ground observational site.

[c]5, 10, 30 and 60 are the temporal averaging windows ($\Delta T = \pm$ 5, 10, 30 and 60 minutes) around OMI overpass time.

Atmos. Chem. Phys. Discuss., https://doi.org/10.5194/acp-2018-720
Manuscript under review for journal Atmos. Chem. Phys.
Discussion started: 3 September 2018

Atmospheric Chemistry and Physics Discussions

Table 5. Same as Table 4 but for evaluating OMI Noon_FS EDR.

statistics	D = 50				D = 25	D = 10
	5 min	10 min	30 min	60 min	5 min	5 min
N	100696	100725	100773	100841	67530	17442
R	0.88	0.89	0.90	0.91	0.87	0.87
Slope	0.87	0.89	0.92	0.95	0.88	0.89
Intercept	25.6	23.7	20.9	18.8	25.4	24.8
MB	10.1	10.2	10.9	13.2	10.4	10.7
RMSE	42.2	40.8	38.7	37.5	43.3	43.2

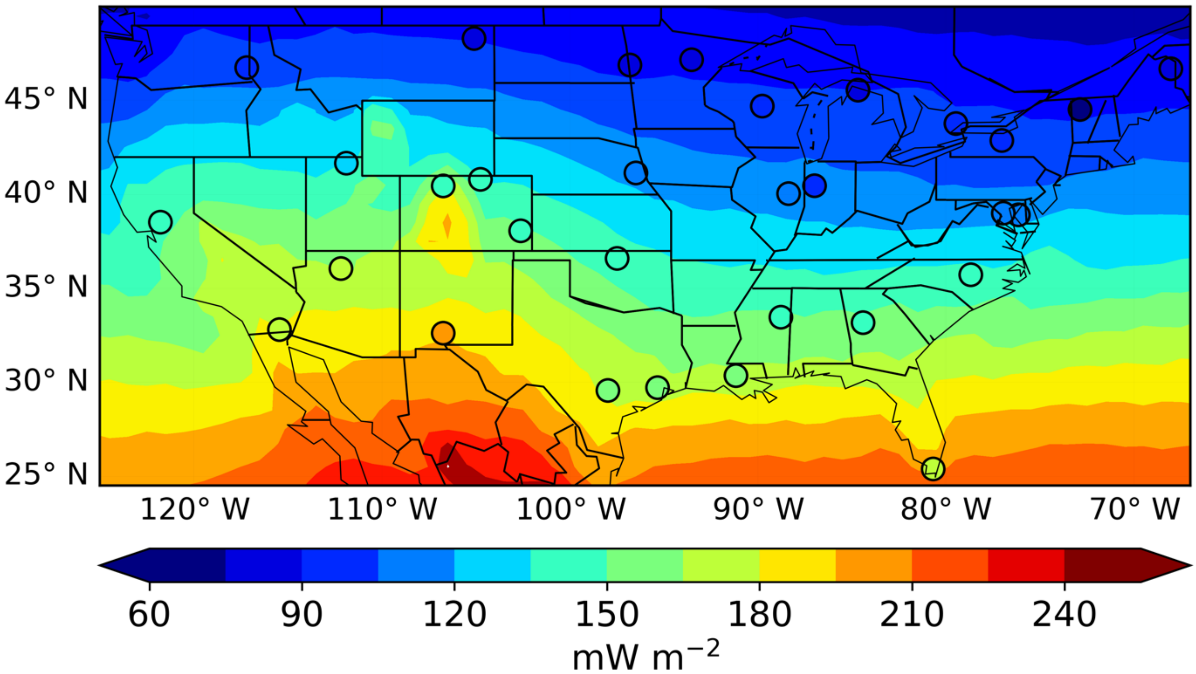

Figure 1: Map of OMI level 3 EDR (mW m^{-2}) at solar noon time under full-sky conditions averaged over 2005–2017, overlaid with 31 ground observational sites averaged over 2005–2017 around solar noon time with ΔT = ±5 minutes.

Atmos. Chem. Phys. Discuss., https://doi.org/10.5194/acp-2018-720
Manuscript under review for journal Atmos. Chem. Phys.
Discussion started: 3 September 2018

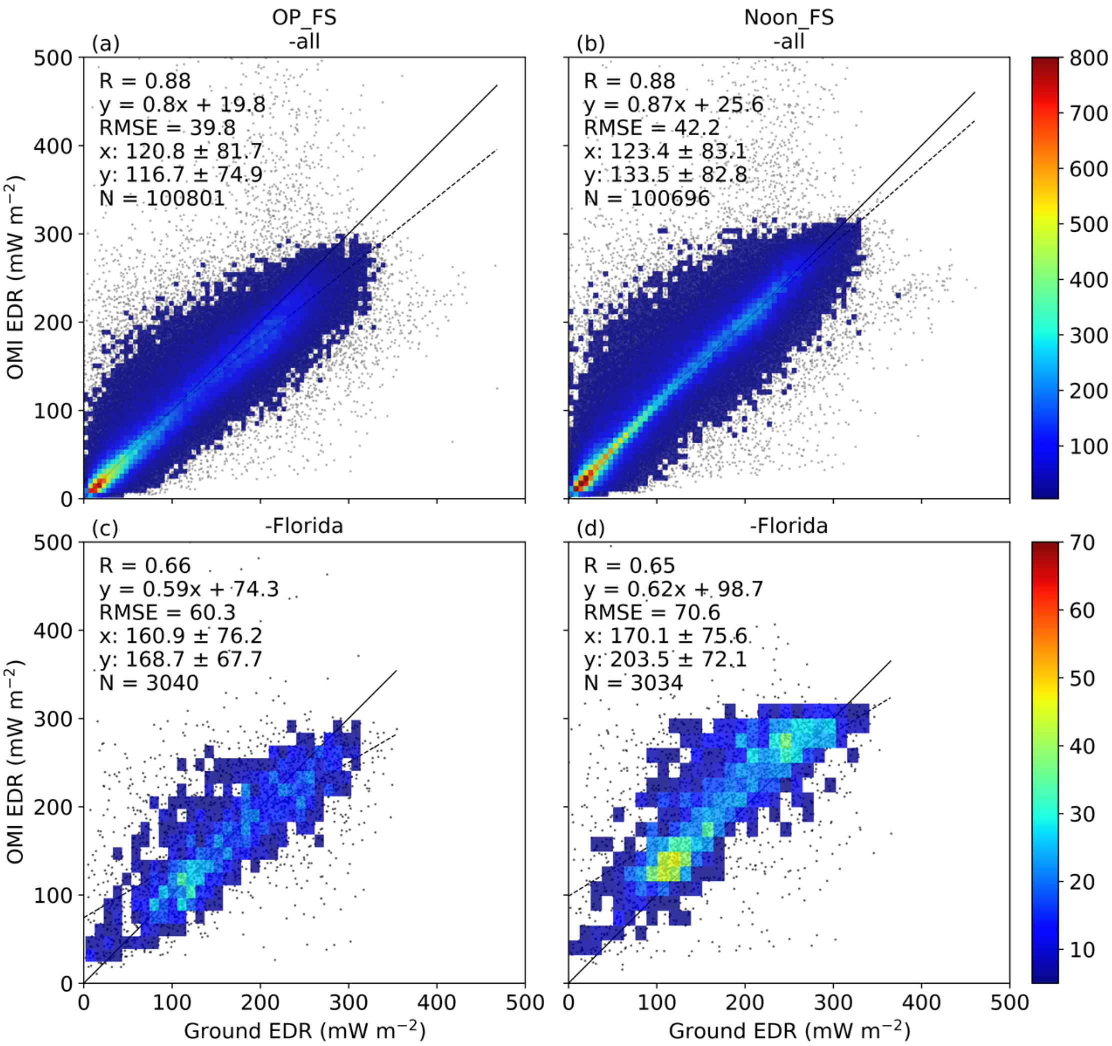

Figure 2: Scatter plots of OMI EDR data with ground observations from year 2005 to 2017. (a) and (b) show the comparisons of OMI OP_FS and Noon_FS EDR with measurements at all of the 31 ground observational sites, respectively, while (c) and (d) only show the comparisons of OMI EDR with ground measurements at Homestead, Florida (FL01). In each scatter plot, also shown is the correlation coefficient (R), the root-mean-square error (RMSE), the number of collocated data points (N), the density of points (the color bar), the best-fit linear regression line (the dashed black line) and the 1:1 line (the solid black line).

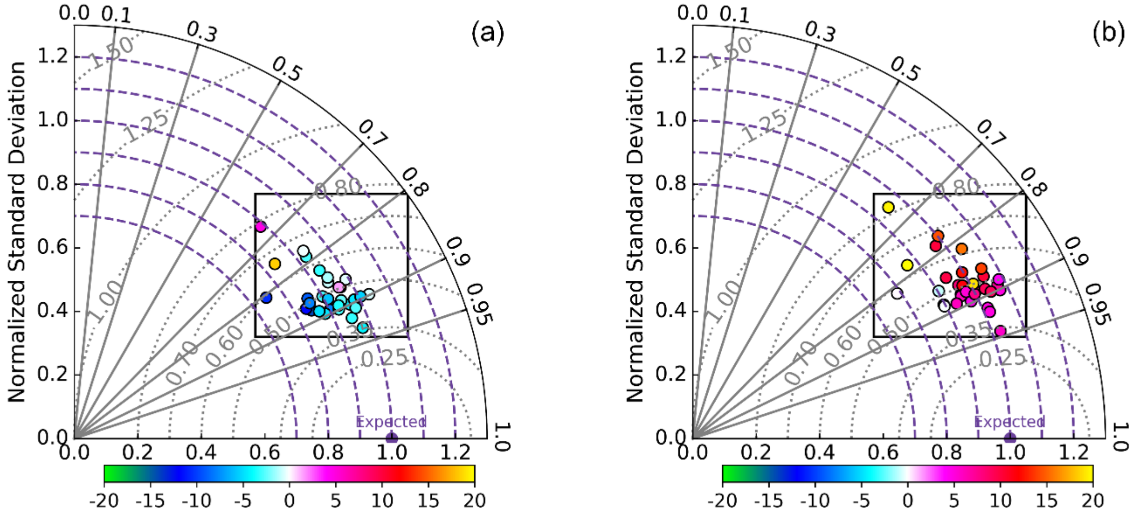

Figure 3: Taylor Diagrams for evaluating OMI OP_FS EDR (a) and Noon_FS EDR (b) against 31 ground observational sites matched with D = 50 km and ΔT = ±5 minutes, respectively. The circles represent the ground sites and the color at each circle represents the NMB (%).

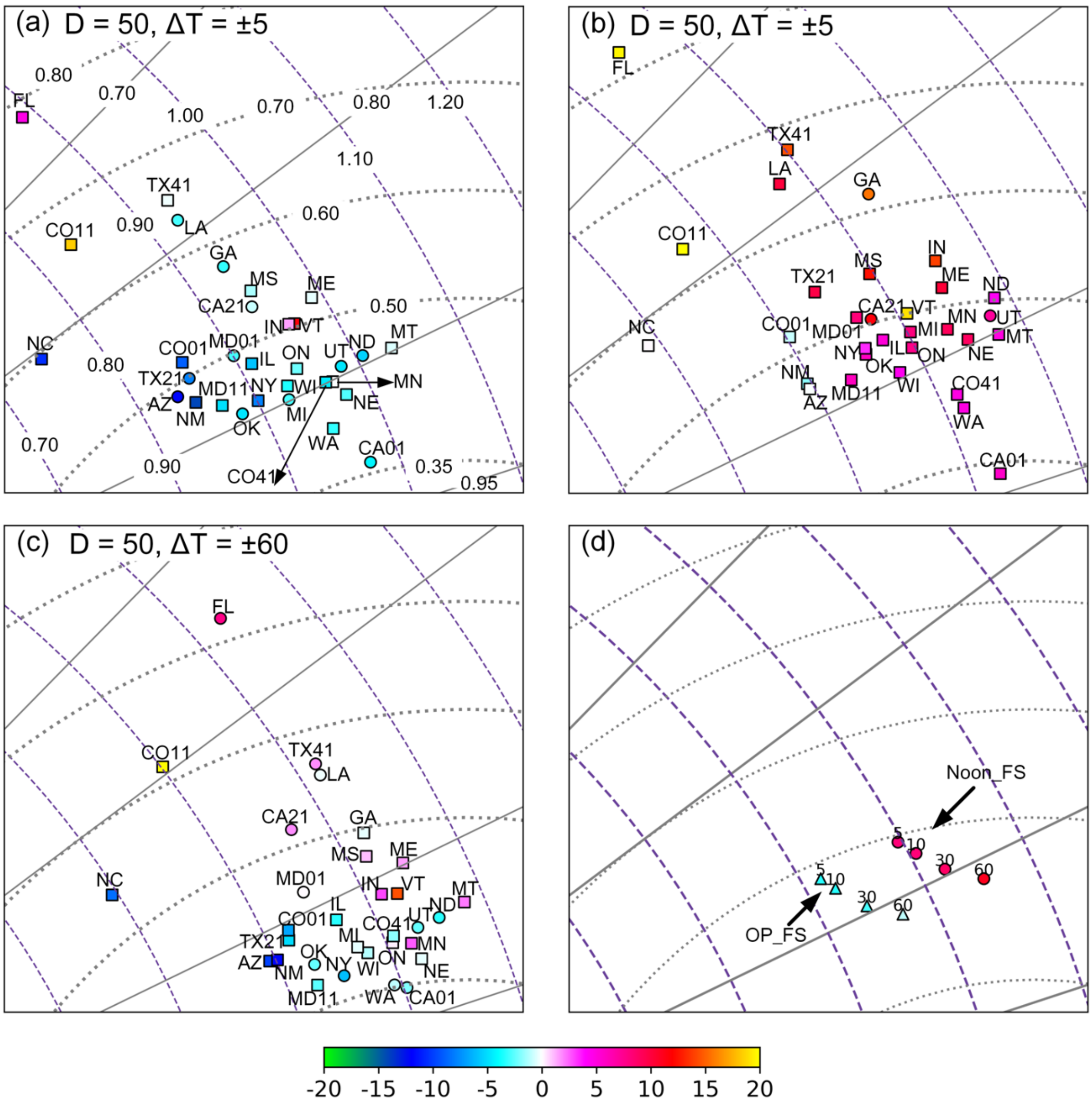

Figure 4: (a) and (b) are zoomed-in plots corresponding to the areas in the black box in Fig. 3(a) and Fig. 3(b), respectively. (c) is the zoomed-in plot for the evaluation of OMI OP_FS EDR with D = 50 km and ΔT = ±60 minutes against 31 ground sites. Sites denoted by squares in (a), (b) and (c) have NMB significant at 95% confidence levels. (d) shows the evaluation of OMI OP_FS EDR (triangles) and Noon_FS EDR (circles) with D = 50 km and ΔT = ±5, 10, 30 and 60 minutes against the ensemble of 31 ground observational sites.

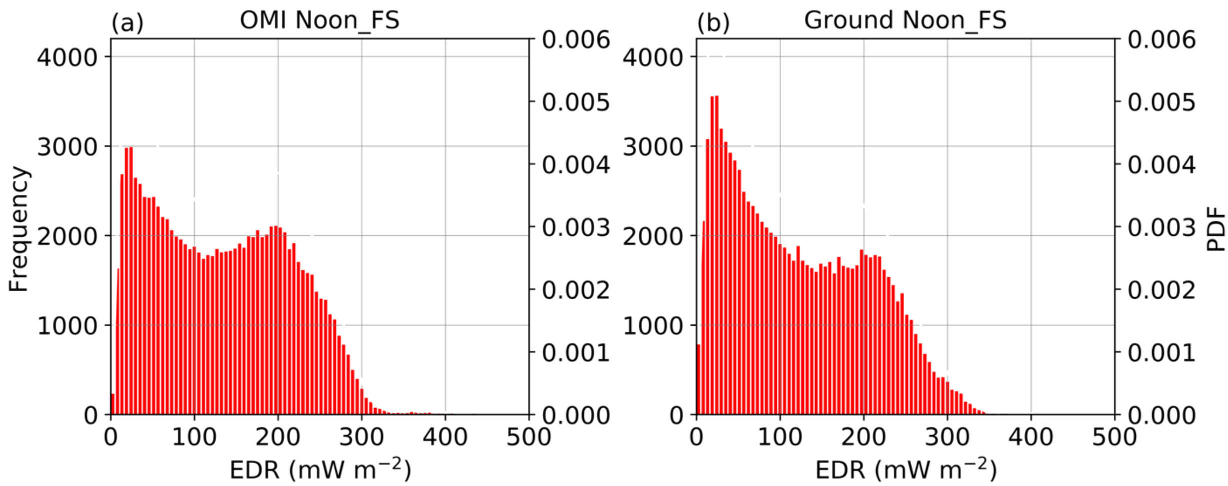

Figure 5: Frequency (left axis) and PDF (right axis) of the surface EDR at the solar noon time for OMI (a) and 31 ground observational sites (b) for year 2005–2017. All the data pairs are matched with D = 50 km and ΔT = ±5 minutes.

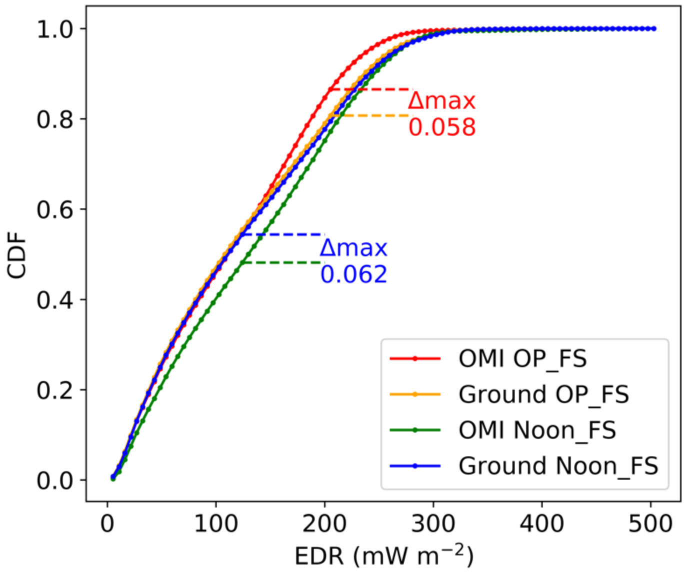

Figure 6: Cumulative distribution functions (CDFs) of surface EDR from both OMI and 31 ground observational sites over 2005–2017. The maximum differences between OMI and ground observational CDFs are shown in the horizontal dashed lines and their values are shown as the labels.

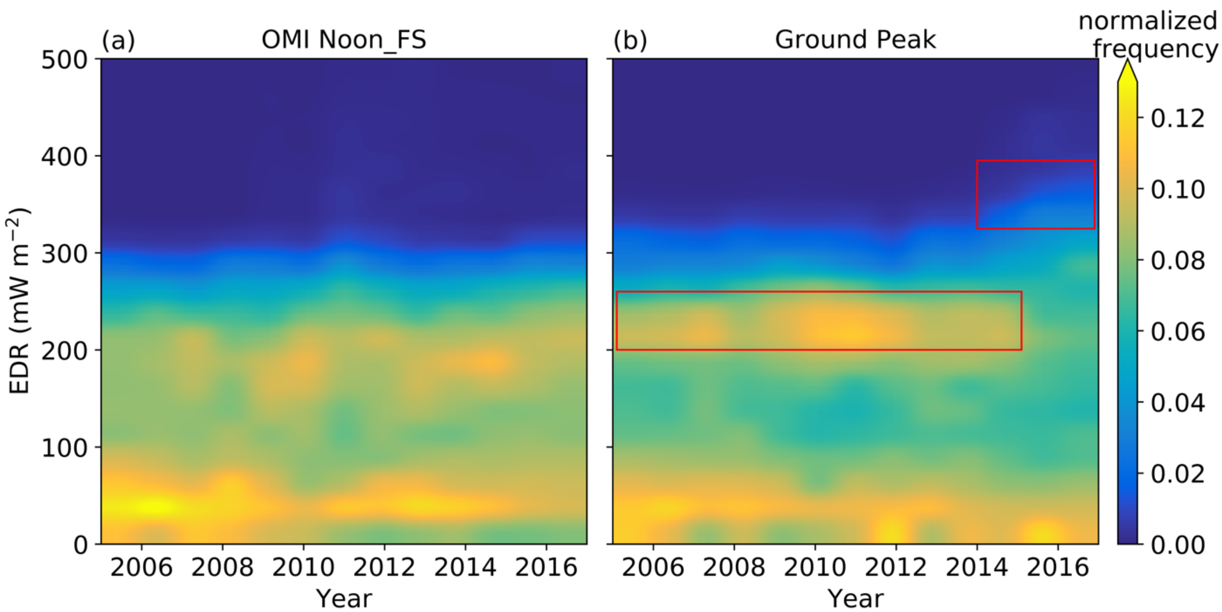

Figure 7: Contour plot of normalized frequency of surface EDR from OMI Noon_FS (a) and ground peak (b) for 31 ground sites. The ground peak refers to the highest dose rate found in a day at each site. The normalized frequency is calculated as follows: first, the surface EDR from both OMI and ground observation are binned by 25 mW m^{-2} for each year and then normalized by the total number of data points for each year. A smooth effect at the contour line was also performed. The red box on the top in (b) marks the areas where the ground peak EDR started to increase after staying consistent from 2005 to 2014 and the red box on the bottom shows the high frequency occurrence areas of ground peak EDR.

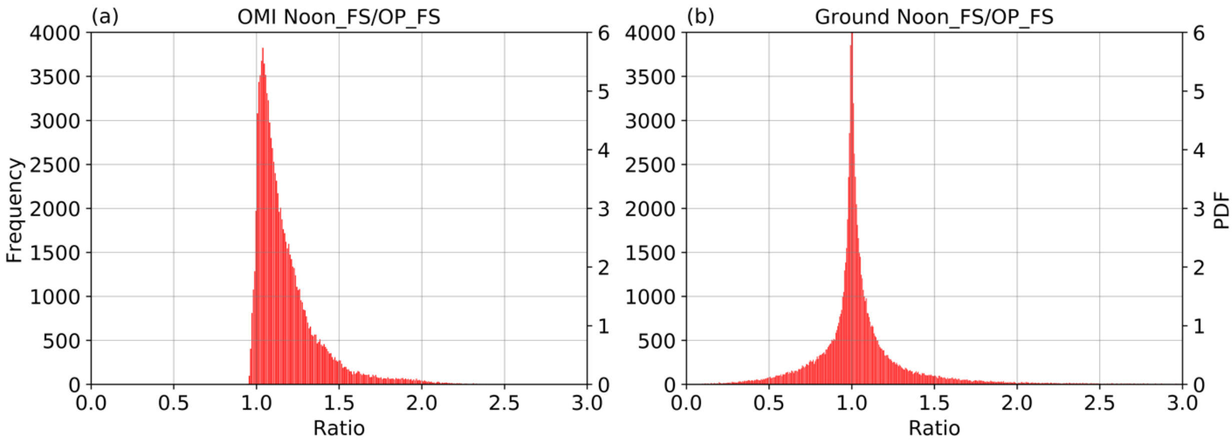

Figure 8: Frequency (left axis) and PDF (right axis) of the EDR ratio of Noon_FS/OP_FS. (a) and (b) are for the OMI and ground ratio respectively. All the data pairs are matched with D = 50 km and ΔT = ±5 minutes for the 31 ground sites.

Atmos. Chem. Phys. Discuss., https://doi.org/10.5194/acp-2018-720
Manuscript under review for journal Atmos. Chem. Phys.
Discussion started: 3 September 2018

Atmospheric Chemistry and Physics
Open Access
Discussions

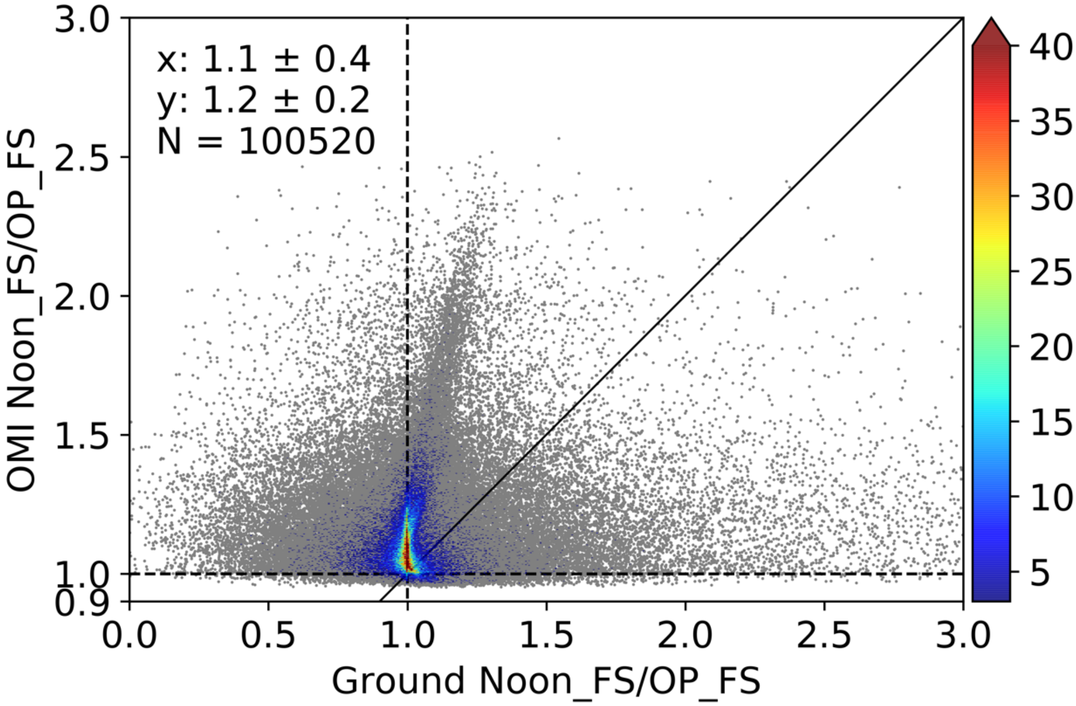

Figure 9: Scatter plot of EDR ratio of Noon_FS/OP_FS from OMI and the ratio from ground measurements for 31 sites. All the data pairs are matched with D = 50 km and ΔT = ±5 minutes. Also shown on the scatter plot is the number of collocated data points (N), the density of points (the color bar), and the 1:1 line (the solid black line). Note the scale difference between x-axis and y-axis.

Atmos. Chem. Phys. Discuss., https://doi.org/10.5194/acp-2018-720
Manuscript under review for journal Atmos. Chem. Phys.
Discussion started: 3 September 2018

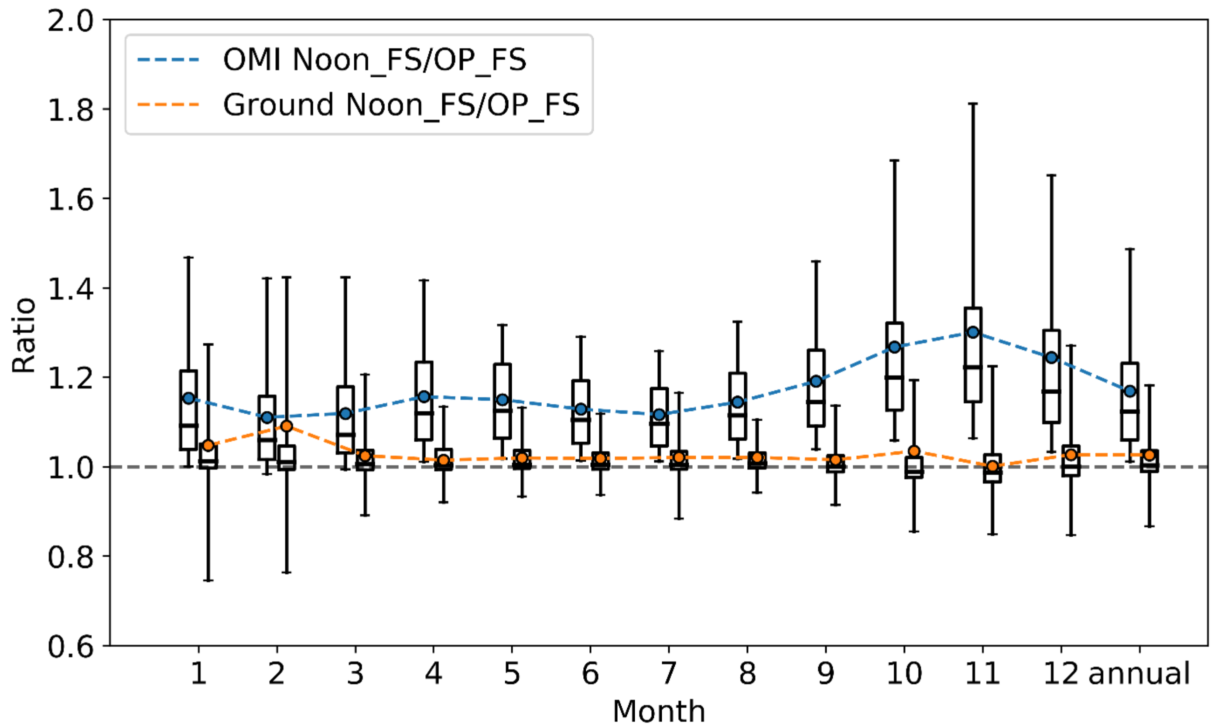

Figure 10: Monthly EDR ratio of Noon_FS/OP_FS EDR from OMI (blue) and the ground (orange) for the 31 sites. The box-whisker plots show the 5th and 95th percentiles (whisker), the interquartile range (box), the median (black line) and the mean (the dots).

Atmos. Chem. Phys. Discuss., https://doi.org/10.5194/acp-2018-720
Manuscript under review for journal Atmos. Chem. Phys.
Discussion started: 3 September 2018

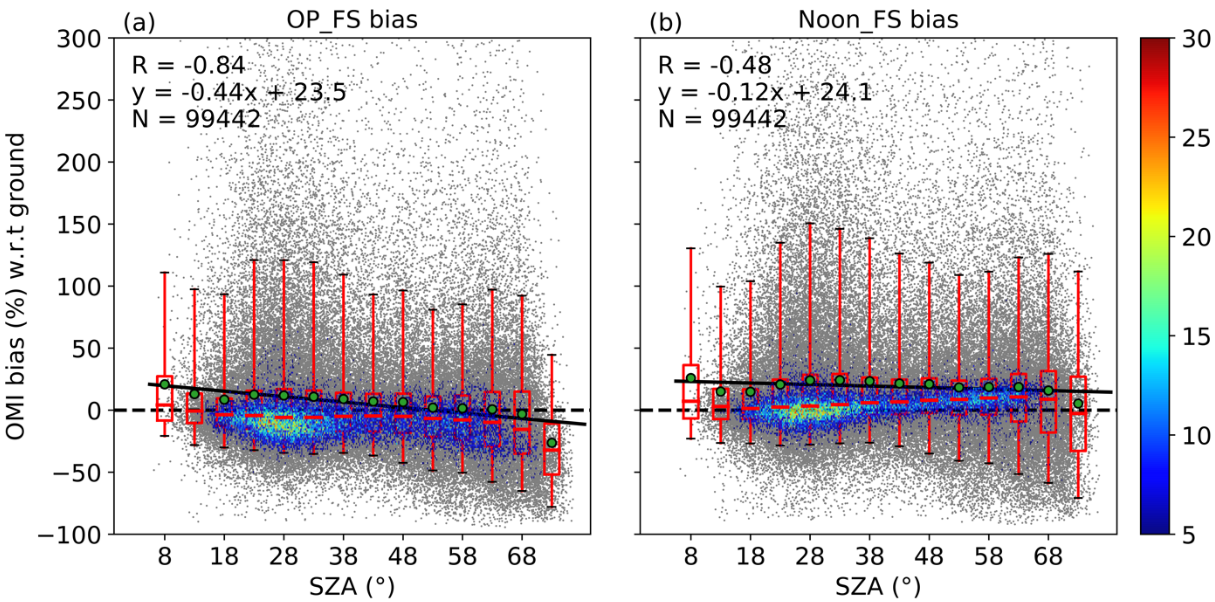

Figure 11: Scatter plot of the relative bias (%) between OMI and ground observational EDR and the OMI overpass time SZA. (a) and (b) are for OP_FS and Noon_FS EDR comparison respectively. All the data pairs are matched with D = 50 km and ΔT = ±5 minutes for the 31 ground sites. The box-whisker plot of the bias is based on the binned SZA using a bin size of 5º. The box-whisker plots show the 5th and 95th percentiles (whisker), the interquartile range (box), the median (red line) and the mean (green dots). Also shown on the scatter plot is the number of collocated data points (N), the density of points (the color bar), the best-fit linear regression line (the solid black line), the regression equation and the correlation coefficient (R). Note that the linear regression is performed between the bin averaged bias and SZA.

Atmos. Chem. Phys. Discuss., https://doi.org/10.5194/acp-2018-720
Manuscript under review for journal Atmos. Chem. Phys.
Discussion started: 3 September 2018

Atmospheric Chemistry and Physics
Open Access
Discussions

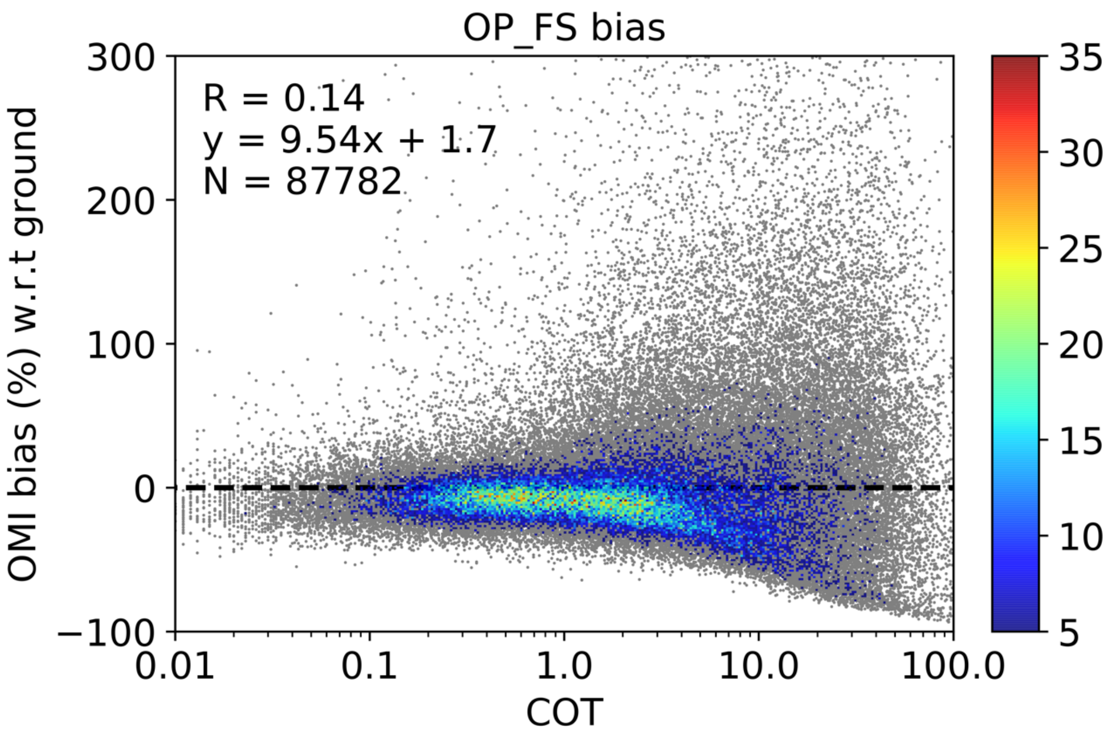

Figure 12: Scatter plot of the relative bias (%) between OMI OP_FS and ground observational EDR and the OMI retrieved COT (360 nm) for the 31 ground sites. Also shown on the scatter plot is the number of collocated data points (N), the density of points (the color bar), the regression equation and the correlation coefficient (R).

Atmos. Chem. Phys. Discuss., https://doi.org/10.5194/acp-2018-720
Manuscript under review for journal Atmos. Chem. Phys.
Discussion started: 3 September 2018

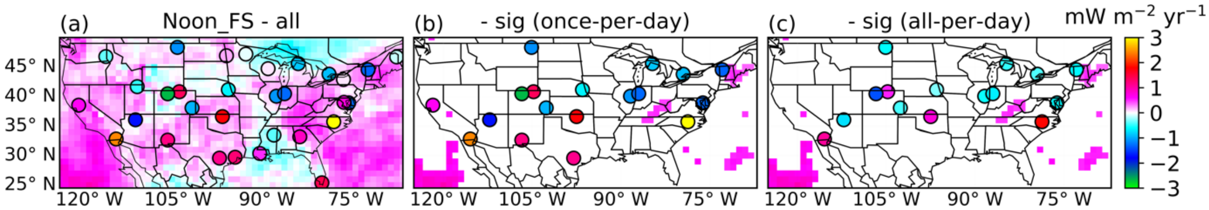

Figure 13: (a) is the distribution of the OMI level 3 solar noon time full-sky EDR trend over 2005–2017 overlaid with the trend at 31 ground observational sites calculated with D = 50 km and ΔT = ±5 minutes around local solar noon time. (b) is the same as (a) but only showing the areas and sites that are significant at the 95% confidence level. (c) shows the distribution of the trend at ground sites (significant at the 95% confidence level), computed with D = 50 km and temporally averaging all the data available in a day.

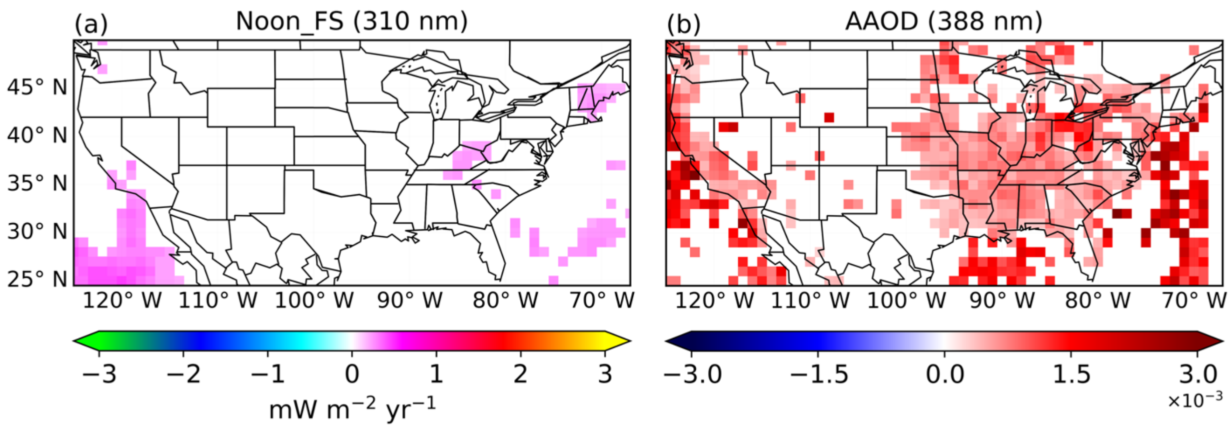

Figure 14: Map of trend derived from OMI level 3 solar noon time full-sky EDR at 310 nm (a) and level 3 AAOD at 388 nm (b) over 2005–2017. Shown are significant regions at the 95% confidence level.

Atmos. Chem. Phys. Discuss., https://doi.org/10.5194/acp-2018-720
Manuscript under review for journal Atmos. Chem. Phys.
Discussion started: 3 September 2018

Atmospheric Chemistry and Physics
Open Access
Discussions

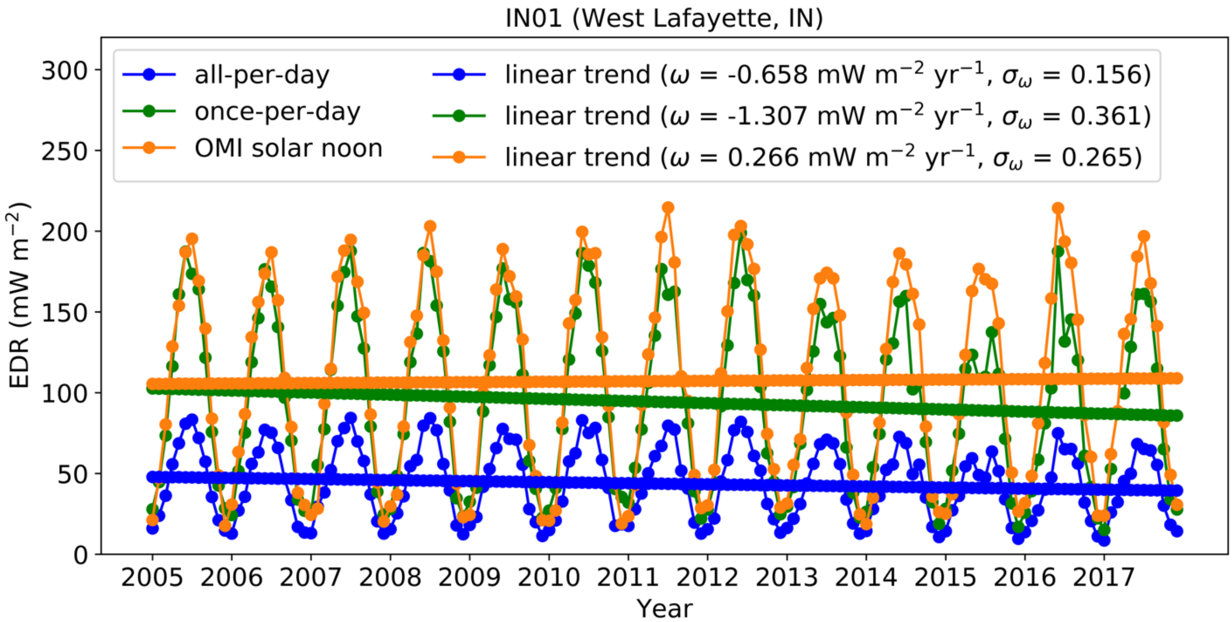

Figure 15: Time series (dotted lines) of monthly OMI level 3 solar noon time full-sky EDR (orange) and ground observational EDR from 2005–2017 using once-per-day (green) and all-per-day (blue) sampling method for site IN01. The once-per-day sampling collects EDR data around local solar noon time while the all-per-day averages all the EDR data in a day. The straight lines are the linear trends derived from Eq. (5).